ABSTRACT

Title: POLARIZATION-PRESERVING WAVEGUIDE FILTER FOR ASTRONOMICAL APPLICATIONS

Felice Maria Vanin, Master of Science, 2005

Directed By: Professor Kawthar Zaki
Department of Electrical Engineering

As part of NASA's Beyond Einstein Program, the characterization of the Cosmic Background polarization has become a high priority for NASA. Since 2002, the efforts in which NASA is engaged are the first steps in the development of the instrumentation to achieve this vision. The critical systems that have previously caused the most losses have to be replaced. Microwave waveguide components are ideal to replaces old systems, improving accuracy of measurement and reducing the losses. In this work, a novel microwave waveguide filter and transformer are presented and discussed. The filter has been designed with 30% fractional bandwidth, guaranteeing extreme stop-band performances by using a quadruple ridge waveguide cross section. The waveguide component exhibits four-fold-symmetry preserving the dual polarization state of the electromagnetic field and resulting ideal for astronomical detections. Moreover, the important suppression of the fundamental mode re-resonance by using attenuation zeros is also discussed.

POLARIZATION-PRESERVING WAVEGUIDE FILTER FOR ASTRONOMICAL APPLICATIONS

by

Felice Maria Vanin

Thesis submitted to the Faculty of the Graduate School of the
University of Maryland, College Park, in partial fulfillment
of the requirements for the degree of
Master of Science in Electrical
Engineering
2005

Advisory Committee:

Professor Kawthar Zaki, Chair
Professor Christopher Davis
Professor Julius Goldhar

Dedication

To my wonderful parents and to my brother…

Citations

"Data la causa, la natura
opera l'effetto nel più
breve modo che operar
si possa"

Leonardo da Vinci

"Verae amicitiae sempiternae sunt"

Cicerone

Acknowledgements

This work is dedicated to all the people that supported me in my Fulbright experience in the United States.

I want to thank especially Mr. James Andary from NASA-Goddard Space Flight Center, where I have worked during the summer; this work would not have been produced without his sincere and necessary interest. I want to thank Dr. Dietmar Schmitt from the European Space Agency who has been my mentor and friend for many years and who has been an essential support during the development of this work.

A very special thanks to Dr. Edward J. Wollack from NASA/GSFC who has been supervisor of this work. I appreciate the opportunity of working with him, as it was a great pleasure to be part of his research group in Goddard. A special thanks also for Mrs. Cathy Long from the Microwave and Technology Branch in NASA/GSFC for being such a nice and wonderful person. I cannot wish a better branch head. Thanks to my great advisor Dr. Kawthar Zaki and to her fantastic advices. Thanks also to Mr. Fabrizio De Paolis from ComDev Canada for technical consulting. Thanks also to Dr. Ali Atia, Dr. Saad, and Dr. Ralph Levy for their inspirations and useful discussions.

I want to thank Dr. Jud Samon who helped me so much in the United States since my arrival. Thanks to Mr. John Mollish from the University of Maryland and his immense patience.

I want to thank all of my friends in Italy, Holland, France, Spain, England, and all of my new friends in America.

Thanks also to the Fulbright program and to NASA/Goddard Space Flight Center for giving so many opportunities.

Thanks a lot to my wonderful parents in Roma and to my older brother.

Table of Contents

Chapter 1 – Cosmology and filters

Evidence of the birth of our universe was first detected still hanging around in our atmosphere way back in 1965 when the young radio astronomers Arno Penzias and Robert Wilson desperately tried to get rid of background noise picked up by their communications antenna at the Bell Laboratories at Homdel, New Jersey. Upon finally asking for advice on how to get rid of their noise, the men learned that they were not listening to cracks in the seams of their dishes and dusty circuits, but to the "birth" of the universe, the Big Bang. Penzias and Wilson won the 1978 Nobel Prize in Physics. Nevertheless, science would need multiple decades of investigation before the Big Bang became an established theory.

Realizing that they were the first to listen to the whispers of the early universe must have been an extraordinary experience for the two young radio astronomers, but *seeing* the first picture of the "birth" of the universe was likely to have been an equally extraordinary experience for NASA's Goddard Space Flight Center during NASA's 1989 Cosmic Background Explorer (COBE) mission.

COBE became the first satellite dedicated to the study of the whole of the universe and man's place in it by measuring cosmic background radiation lingering from the Big Bang. NASA's focus on finding cosmic infrared background radiation, mapping the cosmic radiation, and comparing the spectrum of the cosmic microwave background radiation with a precise blackbody led to major cosmologic discoveries, including our universe's baby picture. Of course the first image NASA presented from COBE's mission looks like blobs of Kelvin temperatures, but scientist's worldwide were astonished as they looked into the blobs and saw what a group of American scientists described on April 23, 1992 as the primordial "seeds" (CMBE anisotropy) of the universe. The announcement of the discovery spread worldwide and COBE's findings were recognized as a fundamental scientific discovery.

Fig. 1-1: COBE science mission logo.

Knowing that the light that was reaching the COBE satellite had been stretched out as the universe had stretched, we also know that light that was once beyond gamma rays is now reaching us in the form of microwaves. COBE confirmed that the microwaves created by the Big Bang are there, that they can be mapped, and that the radiant energy of the birth of the universe was released within only a year's time, a relatively

short birth for a universe containing more than ten billion trillion planets. COBE's images were indeed revolutionary, and they gave NASA a direction to follow in the further investigation into the beginnings of the universe.

NASA maintained its focus and created the Wilkinson Microwave Anisotropy Probe (WMAP), named in honor of David Todd Wilkinson, a world-renowned pioneer in the field of cosmology specializing in the study of the Cosmic Microwave Background radiation (CMB) left over from the Big Bang. If COBE's image were our universe's first Polaroid, the WMAP or "MAP" image would be our universe's first digital photo.

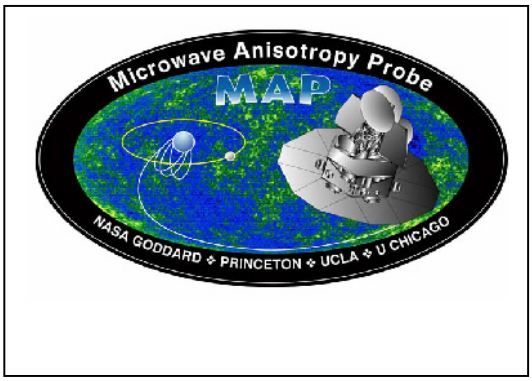

Fig. 1-2: MAP science mission logo.

MAP's goal follows COBE's direction: To determine the geometry, content, and evolution of the universe. The major scientific aim of the satellite's mission was to prove that the relative Cosmic Microwave Background (CMB) temperature could be measured accurately over the full sky with high angular resolution and sensitivity. NASA knew that they needed to control systematic errors in the final maps, so they narrowed their specific goals to the following: to map the relative CMB temperature over the full sky with an angular resolution of at least 0.3°, a sensitivity of

20 μK per 0.3° square pixel, with systematic artifacts limited to 5 μK per pixel. MAP resolves slight temperature fluctuations, which vary by only millionths of a degree.

On June 30, 2001, MAP launched aboard a Delta II-7425-10 vehicle from sunny Florida's Kennedy Spaceflight Center for a three-month journey to an L2 orbit. By April 2002, MAP completed it's first full sky observation, and the beauty of MAP's observations is in their levels of detail. The results of the MAP image provide an astonishingly accurate map of temperature fluctuations in the first detailed full sky picture of the oldest light in the universe which strengthen and support the Big Bang and Inflation theories, reminding us again of names like Einstein and Hubble.

The first results? Like Einstein predicted, the universe is indeed flat. Of course Albert's other theory, the cosmological constant, what science often calls "his greatest blunder," wasn't a blunder because he wasn't clever, but most likely because the technology to measure this constant was not available until the Hubble study that theorized an expanding universe. We now know that the universe is not composed of Einstein's cosmological constant that portrays a static universe, but of cosmological parameters that will forever be expanding and accelerating. As a tribute to Einstein, scientists have redefined his cosmological constant as energy density (which is a simplified term for a theory that deserves its' own

thesis work). Furthermore, the MAP mission has filtered down the CMB in order to peer into the narrowest evidence of temperature fluctuations and brightness of the ancient lights of the universe, supporting both the Big Bang and Inflation theories. Though it is, to the average listener, somewhat more exciting to talk about the filtering out of signals from, say, the galactic dust that can skew results, I will now get into some of the reasons why MAP has given scientists the advantage of looking at the most noise-free data.

One factor yet to be defined in this work is that of the “A” in MAP, anisotropy: the difference in the property of a system with changes in direction. The MAP mission’s instruments allowed for the most accurate picture of differences between measurements taken from different directions. The instrumentation consists of a set of passively cooled microwave radiometers with 1.4 x 1.6 meter diameter primary reflectors to provide the desired angular resolution. Measuring the temperature of the microwave sky to an accuracy of one millionth of a degree requires careful attention to possible sources of systematic errors. The avoidance of systematic measurement errors drove the design of WMAP.

An integral part of avoiding systematic errors is to pay close attention to the separation of Galactic foreground signals from the cosmic background radiation. When we are talking about signals, what we are

really talking about is frequency. The MAP specification called for equal noise sensitivity per frequency band of ~35 μK per 0.3° x 0.3° square pixel, and these specifications were achieved after two years of careful observations of five main frequency bands. The following table gives the specified sensitivity for each of the five WMAP frequency bands:

WMAP Sensitivity (μK, 0.3° x 0.3° pixel)

Frequency	22 GHz	30 GHz	40 GHz	60 GHz	90 GHz
Specification	~35	~35	~35	~35	~35

In short, this specified sensitivity to noise, combined with optics, receivers, angular resolution, and specified coverage of frequencies, the Map mission gathered the facts that outline a new unified understanding of the universe. Including the conclusion that the universe is flat, here are the MAP results:

- Universe is 13.7 billion years old, with a margin of error of close to 1%.
- First stars ignited 200 million years after the Big Bang.
- Light in WMAP picture is from 379,000 years after the Big Bang.
- Content of the Universe:
    - 4% Atoms, 23% Cold Dark Matter, 73% Dark Energy.
    - The data places new constraints on the Dark Energy. It seems more like a "cosmological constant" than a negative-

pressure energy field called "quintessence". But quintessence is not ruled out.

- Fast moving neutrinos do not play any major role in the evolution of structure in the universe. They would have prevented the early clumping of gas in the universe, delaying the emergence of the first stars, in conflict with the new WMAP data.
- Expansion rate (Hubble constant) value: Ho= 71 (km/sec)/Mpc (with a margin of error of about 5%)
- New evidence for Inflation (in polarized signal)
- For the theory that fits our data, the Universe will expand forever. (The nature of the dark energy is still a mystery. If it changes with time, or if other unknown and unexpected things happen in the universe, this conclusion could change.)

With this type of result, NASA has certainly been inspired to continue the investigation into the birth of the universe. As mentioned above, science has an updated account of the age of the universe, 13.7 billion years old, which is now accepted worldwide. But, just as the age of the universe has previously been a nagging mystery to the science community, the mystery lives on in spite of NASA's youngest image of the universe, a snapshot at a mere 379,000 years old. As you may guess, the new mission? The aim will be to look even further back in time, to find even earlier lights, an earlier picture of our universe.

And looking back in time will certainly require a powerful and noiseless lens, a lens with unfathomably clear focus. Just as Ansel Adams has given the world the purest tones black and white known to photography through his masterful use of filters, NASA plans to master its use of filter technology in order to see the purest photo of the early universe to date.

Chapter 2 – Basics of filter theory and network modeling

The first work on microwave filters commenced before World War II; in particular, W. P. Manson and R.A. Sykes [2-1] published the first significant paper in 1937 and much of the foundation of modern filter theory took place during that time. Some years later, a book written by Matthaei, Young, Jones [2-2] was widely accepted and soon was (and still is) considered the bible in filter design studies. Cohn and Levy [2-3], [2-4] carried the baton of filter study further by making important contributions in the 1960's. It was finally technology that grabbed the torch during the 80's when Electromagnetic CAD tools [2-5] established applications that are more modern improving accuracy in the design techniques. This chapter introduces some basics of filter theory using concepts and results offered by these authors. A description of the different types of filters, Chebyscheff theory and network concepts are also given. In fact, network models are the basic for filter designs before using advanced electromagnetic simulation tools.

2.1. Filter types

In the following paragraph, the basic types of filters are briefly described and a comparison is made between an ideal rectangular filter response and a realizable response; some of the parameters and functions used in this work are also defined.

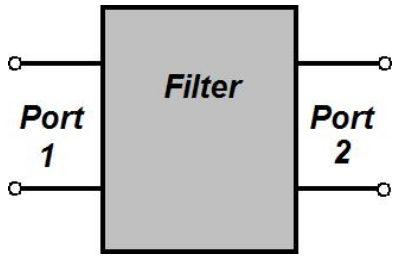

Fig.2-1: A filter as a 2-port network

'A filter is a linear 2-port element devoted to furnish a signal to the second port, the spectrum of the signal is so well transformed by the filter from the first port to the second one'.

Fig.2-1 shows a filter as a 2-port network. There are four main types of filters: lowpass filter, highpass filter, bandpass filter and stopband filter. Lowpass filters allow only low frequency signals to be transmitted from the input port to the out port, highpass filters allow high frequency signals to be transmitted and therefore it has the opposite behavior. Bandpass filters allow only a restricted range of frequencies to be transmitted and this range is specified between lower and upper frequency points. Stopband filters allow all the frequencies to be transmitted except for a specified range.

The ideal rectangular attenuation behavior of these four kinds of filters is depicted in Fig. 2-2 versus normalized frequency.

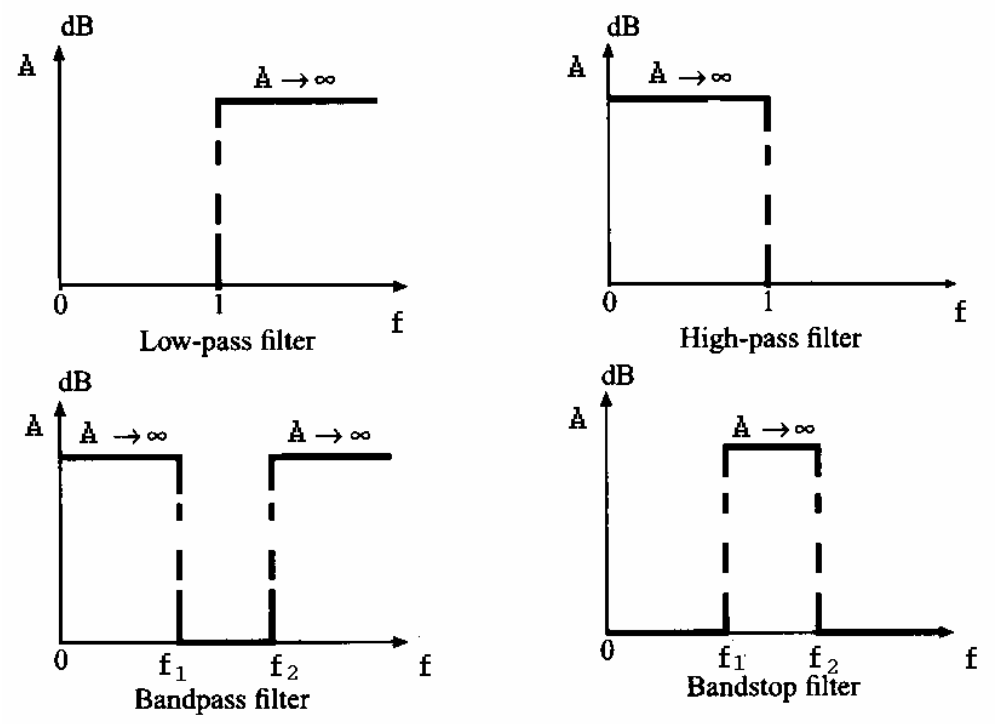

Fig. 2-2: Ideal attenuation profiles of lowpass, highpass, bandpass and stopband filters

Every procedure, which has as the aim of designing and developing a filter, begins with the specifications in a detail of the attenuation profile $A(\omega)$ or of the transmission profile $T(\omega)$. The latter is the defined as the inverse of $A(\omega)$.

The perfect filter would have, as it can be seen from Fig. 2-2, maximum transmission in the pass-band and zero transmission in the stop-band.

Such filters cannot be realized, so the ideal behavior has to be approximated.

The behavior of a filter is described by its transfer function $T(\omega)$, which is a function of frequency. The function $T(\omega)$ is related to $A(\omega)$ by:

$$A_{dB}(\omega) = 10\,Log_{10}\left(\frac{1}{T(\omega)}\right)$$

A proper choice of the T function defines one of the four types of filters. There are several functions that approximate the ideal behavior. Butterworth, Elliptical, and Chebyscheff are the most known functions. Among them, Chebyscheff polynomials have been selected for the purpose of filter design to obtain the desired transfer function. The Chebyscheff polynomial of degree n, denoted $T_n(x)$, is an n^{th} degree polynomial in x defined as:

$$T_n(x) = \cos\left(n \cdot \cos^{-1}(x)\right)$$

They all oscillate between ± 1 for *x* in the range of | *x* | < *1* and increase in magnitude for *x* outside this range.

Fig. 2-3 gives a sketch of the first five Chebyscheff polynomials.

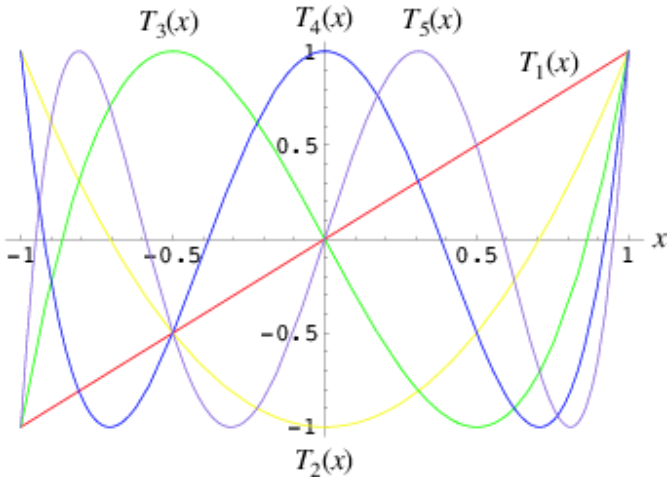

Fig. 2-3: Chebyscheff polynomials.

Using Chebyscheff polynomial, the ideal transfer function response can be approximated. In Fig. 2-4 both responses are compared.

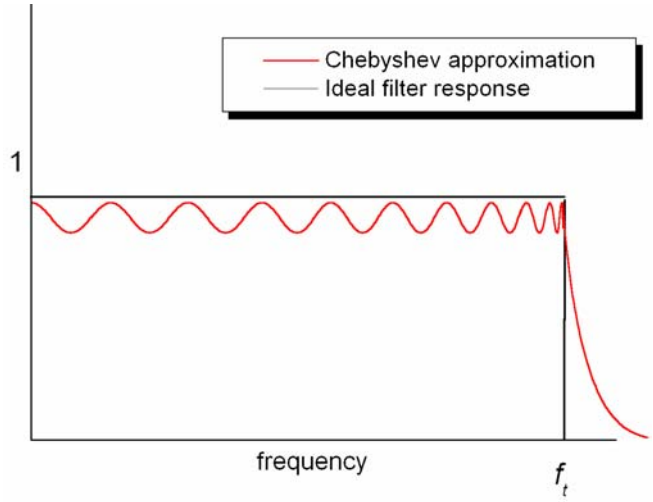

Fig. 2-4: Ideal filter response and Chebyscheff approximation (ε = 0.05, n_f =21).

The ripples characterizing Chebyscheff functions are chosen from the engineer for filter design very small in amplitude. Fig. 2-4 shows the main difference between the two behaviors.

The Chebyscheff transfer function of Fig. 2-4 is given by:

$$(\text{Transfer function})^2 = \frac{1}{1+\varepsilon^2 T_{n_f}^2(x)}$$

where ε defines the amplitude of the ripple. From Fig. 2-4, it can be noted that there is a substantial difference between the ideal lowpass response and the Chebyscheff response. However, the latter function is physically realizable while the first not. Chebyscheff filters also provide an acceptable steepness in the out-of-band attenuation for most practical applications. In Chebyscheff filters, ripples are evident in the bandwidth and it is important to notice that these ripples maintain equal amplitude in the bandwidth.

2.2. Definitions and useful parameters

For microwave applications, it is more desirable to characterize the filter with scattering parameters *S* expressed in dB value. Fig. *2-5* shows a typical response of a filter and some used parameters, which are defined as:

- **Insertion loss** *IL*: The ratio, expressed in dB, of incident power P_{in} to transmitted power P_t**:**

$$IL = 10\,Log_{10}\left(\frac{P_{in}}{P_t}\right)$$

Therefore, the insertion loss is identified as the module of the scattering parameter S_{21} expressed in dB: $20\,Log_{10}\left|S_{21}\right|$.

- **Return loss** *RL* **:** The ratio, expressed in dB, of incident power P_{in} to reflected power P_r :

$$RL = 10\,Log_{10}\left(\frac{P_{in}}{P_r}\right)$$

Consequently, the return loss is identified as the module of the scattering parameter S_{11} expressed in dB: $20\,Log_{10}\left|S_{11}\right|$.

In the case of lossless filters, return loss and insertion loss are related by the well-known conservative energy equation:

$$\left|S_{11}\right|^2 + \left|S_{21}\right|^2 = 1$$

- **Return loss ripple:** The ripple of return loss within the bandwidth as Fig. *2-5* shows.
- **Insertion loss ripple:** The ripple of insertion loss within the bandwidth as Fig. *2-5*.
- **Bandwidth BW**: The bandwidth is defined in Fig. *2-5*, and it is related to the position of the return loss ripples. Therefore, it is called 'equal ripple' bandwidth, analytically expressed from

$$BW = f_2 - f_1$$

where f_2 and f_1 are the edges of the bandwidth.

- **Rejection:** The out-of-band behavior of the filter.
- **Poles:** The zeros of return loss function within the bandwidth.

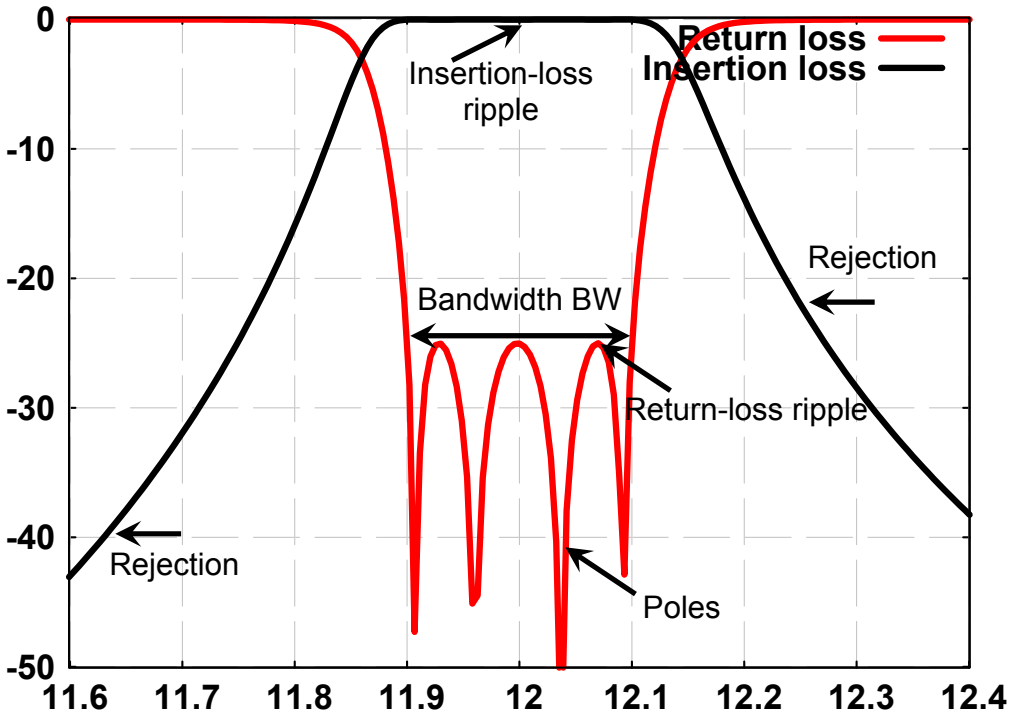

Fig. 2-5: Typical filter response and definitions

2.3. Ripple and filter order in Chebyscheff filters

In many applications, the Chebyscheff response is used since it offers good performances e.g. in terms of rejections and compactness, moreover they are easy to realize with different technologies such a waveguides, strip-lines, or micro-strips. In the following paragraph the

Chebyscheff attenuation function and some other related formulas are defined.

The Chebyscheff attenuation characteristic *A* for lowpass filters is shown in Fig. 2-4 and established as [2-2]:

$$\begin{cases} A_{dB}(\omega') = 10\ L\log_{10}\left(1+\varepsilon\cdot\cos^2\left(n\cdot\arccos\dfrac{\omega'}{\omega_1'}\right)\right), & \omega' \le \omega_1' \\ A_{dB}(\omega') = 10\ L\log_{10}\left(1+\varepsilon\cdot\cosh^2\left(n\cdot\cosh^{-1}\dfrac{\omega'}{\omega_1'}\right)\right), & \omega' \ge \omega_1' \end{cases}$$

The parameter ω' is chosen as a normalized frequency with respect to the angular frequency ω_1', which denotes cut-off frequency for lowpass filters (and the limits of the bandwidth for bandpass filters). The normalized frequency is chosen because it simplifies filter design. In order to choose the attenuation characteristics, it is necessary to value the degree of the filter *n* and the coefficient ε, which is a parameter connected to the insertion loss ripple L_{Ar} in dB. The coefficient ε is given by [2-2]:

$$\varepsilon = 10^{\frac{L_{Ar}}{10}} - 1$$

However, practical requirements specify *return loss* (*RL*) in dB ripple levels and not *insertion loss* ripple. In order to calculate ε, L_{Ar} is given by:

$$L_{Ar} = -10\log_{10}\left(1-10^{\frac{RL}{10}}\right)$$

If for example *RL*=-25 dB (generally indicated with the absolute values, therefore simply 25 dB), L_{Ar}=0.013755 dB and, therefore, ε becomes 0.003172.

The attenuation characteristic becomes steeper if the degree of the filter is increased, so in order to determine properly *n*, a condition on rejection is required for a specified frequency ω_a; the degree *n* of the filter is the minimum *n* that satisfies the following equation:

$$A_{dB}\left(\omega_a'\right) = 10\log_{10}\left(1+\varepsilon\cdot\cosh^2\left(n\cdot\cosh^{-1}\frac{\omega_a'}{\omega_1'}\right)\right)$$

where $\omega_1' = 1$ for normalized lowpass prototype filters.

2.4. Definition of circuit parameter for lowpass prototype filters

Chebyscheff transfer functions can be realized as a ladder network, becoming a model for waveguide structures. Specifically, two circuits for lowpass prototype filters are defined as Fig. 2-6 depicts [2-2]. The network model is the first step in order to calculate the physical dimensions of the filter providing starting values for the design.

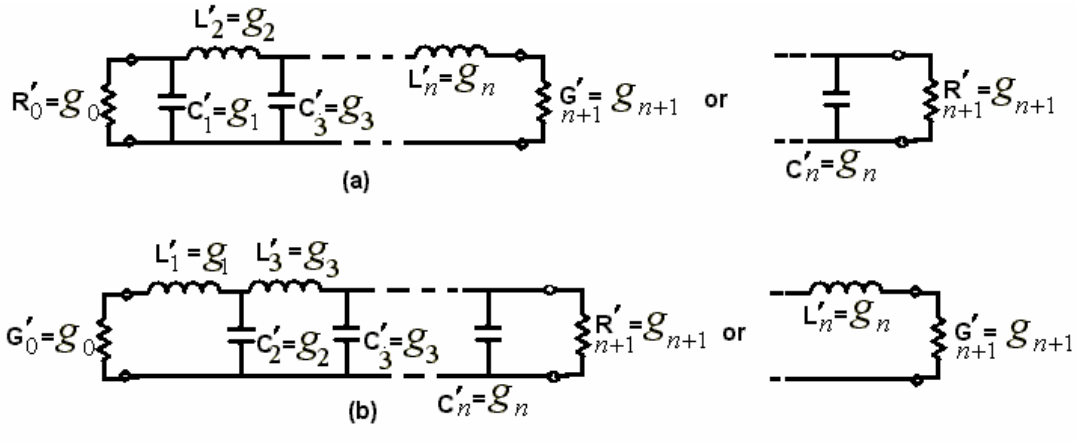

Fig. 2-6: Definition of prototype filter parameters $g_0, g_1, ..., g_{n+1}$

Two possible circuits are shown as (a) and (b), the first is the dual of the second, so there is no difference to use one or the other. The element values $g_0, g_1, ..., g_n, g_{n+1}$ are numbered from 0 to $n+1$, where n is always the order of the filter calculated as above. The elements alternate between series inductance and shunt capacitance as in Fig. 2-6. These elements are defined as [2-2]:

$$g_0 = \begin{cases} \text{Internal generator resistance } R_0' \text{ if } g_1 = C_1' \\ \text{Internal generator conductance } G_0' \text{ if } g_1 = L_1' \end{cases}$$

$$g_n = \begin{cases} \text{The load resistance } R_{n+1}' \text{ if } g_n = C_n' \\ \text{The load conductance } G_{n+1}' \text{ if } g_n = L_n' \end{cases}$$

$$g_k\big|_{k=1...n} = \begin{cases} \text{The inductance for series inductor} \\ \text{The capacitance for a shunt capacitance} \end{cases}$$

The values of the elements of the prototype filter are normalized to have $g_0 = 1$ and $\omega_1' = 1$; however, with simple transformations it is possible to have other impedance values such as follows.

For resistance or conductance:

$$R = \left(\frac{R_0}{R_0'}\right)R' \quad or \quad G = \left(\frac{G_0}{G_0'}\right)G'$$

For inductance:

$$L = \left(\frac{R_0}{R_0'}\right)\left(\frac{\omega_1'}{\omega_1}\right)L' = \left(\frac{G_0'}{G_0}\right)\left(\frac{\omega_1'}{\omega_1}\right)L'$$

For capacitance:

$$C = \left(\frac{R_0'}{R_0}\right)\left(\frac{\omega_1'}{\omega_1}\right)C' = \left(\frac{G_0}{G_0'}\right)\left(\frac{\omega_1'}{\omega_1}\right)C'$$

In these equations, R, L, C, G are related to the scaled circuit, while R', L', C', G' are related to the lowpass normalized circuit. For an n order filter with bandpass ripple L_{Ar}, $g_0 = 1$ and $\omega_1' = 1$ formulas to compute the g elements are given by [2-2]:

$$\begin{cases} \beta = \ln\left(\dfrac{L_{Ar}}{17.37}\right) \\ \gamma = \sinh\left(\dfrac{\beta}{2\cdot n}\right) \\ a_k = \sin\left[\dfrac{(2k-1)\pi}{2\cdot n}\right]\Bigg|_{k=1,\ldots,n} \\ b_k = \gamma^2 + \sin^2\left(\dfrac{k\pi}{n}\right)\Bigg|_{k=1,\ldots,n} \end{cases}$$

and:

$$\begin{cases} g_1 = \dfrac{2a_1}{\gamma} \\ g_k = \dfrac{4a_{k-1}a_k}{b_{k-1}g_{k-1}}\Bigg|_{k=2,n} \\ g_{n+1} = \begin{cases} 1, & \text{for n odd} \\ \coth^2\left(\dfrac{\beta}{4}\right), & \text{for n even} \end{cases} \end{cases}$$

The last equations can be used to calculate the *g* elements of a Chebyscheff filter for a filter of degree n. Therefore, the lowpass prototype filter is defined and frequency transformations can be used in order to "rescale" the frequency response of the prototype filter to the actual use.

Impedance and admittance inverters are often used to transform a lowpass filter composed by capacitance and inductance into another lowpass, which uses inductance or capacitance only. This equivalency

can be performed using *ideal impedance* or *admittance inverters* (see Fig. 2-7).

An impedance (admittance) inverter of impedance (admittance) K (J) is a symmetrical two-port which, looking into its input port, inverts and scales to impedance (admittance) K (J) any impedance Z (admittance Y) connected to its output port.

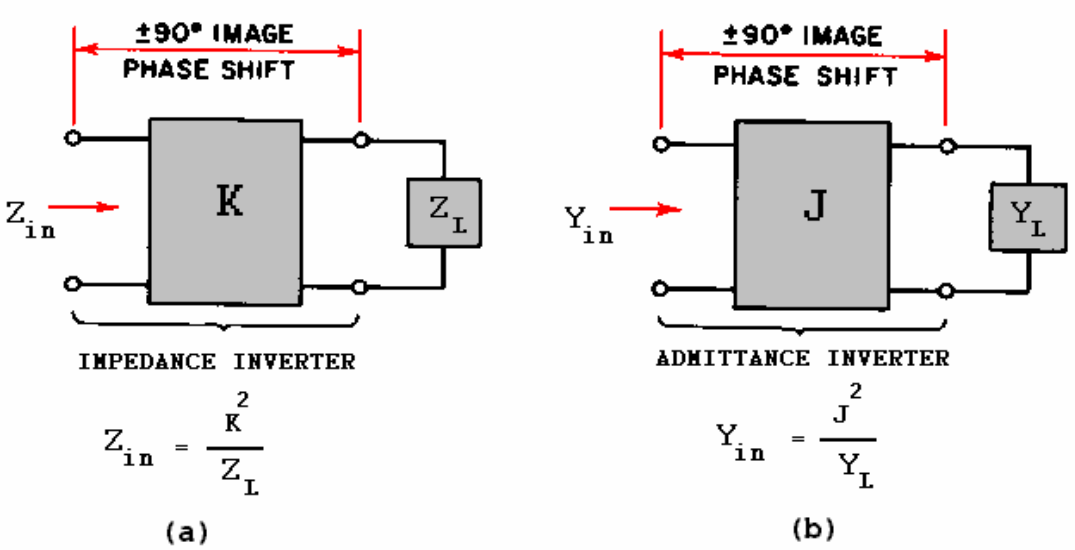

Fig. 2-7: Ideal impedance (a) and admittance inverters (b)

An impedance inverter operates like a quarter-wavelength line of characteristic impedance K at all frequencies; its transfer matrix P is:

$$P = \begin{pmatrix} 0 & iK \\ \frac{i}{K} & 0 \end{pmatrix}$$

If this inverter is terminated in impedance Z_L on one end, the impedance Z_{in} seen looking in from the other side is:

$$Z_{in} = \frac{K^2}{Z_L}$$

An ideal admittance inverter operates like a quarter-wavelength line of characteristic admittance J at all frequencies; its transfer matrix U is:

$$U = \begin{pmatrix} 0 & \frac{i}{J} \\ iJ & 0 \end{pmatrix}$$

It operates like a quarter-wavelength line of characteristic admittance J at all frequencies. If it is terminated in admittance Y_L , the admittance Y_{in} seen looking in from the other side is:

$$Y_{in} = \frac{J^2}{Y_L}$$

It is clear that all networks, which are able to invert impedances, are also able to invert admittances. Therefore, if the inverter is identified with its ABCD matrix, then an impedance inverter with value K is equivalent to an admittance inverter $J = 1/K$.

Because of the inverting action, a series inductance, with an inverter on each side, looks like a shunt capacitance from his exterior terminals and a shunt capacitance, with an inverter on both sides, looks like a series inductance from its external terminals. Making use of these properties, the prototype circuits in Fig. 2-6 can be converted to either of the equivalent forms in Fig. 2-8.

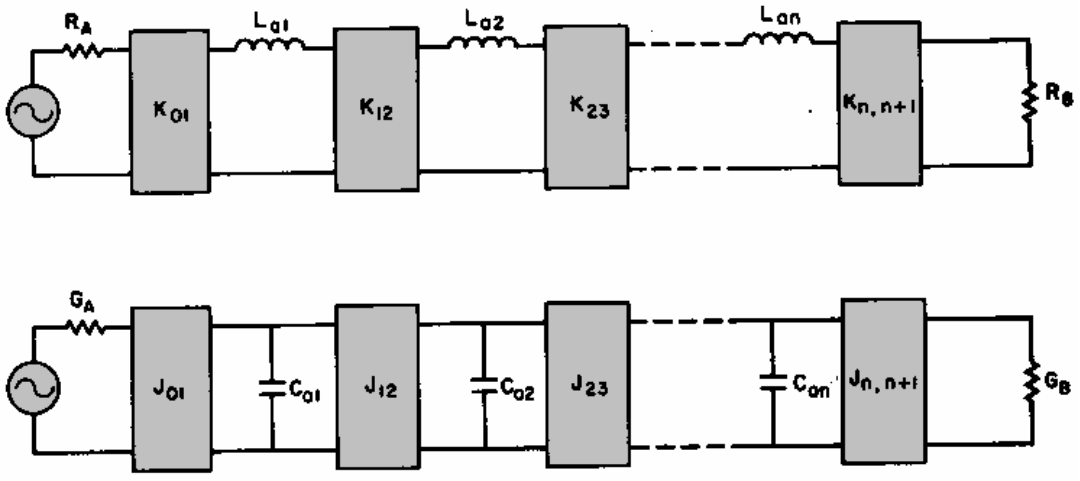

Fig. 2-8: Modified prototype using inverters

The model of Fig. 2-8 has the significant advantage of representing the physical structure of waveguide filters more closely than lamped element models. In fact, the inverters represent the coupling sections and inductances (capacitances) represent the transmissions lines.

2.5. Summary

In this chapter, some initial filter theory has been mentioned, specifically, general classification of the filter types and common terminologies used in filter design. The lowpass Chebyscheff filter design, which is based on normalized frequency, is chosen as a standard model. By using this approach, filter's network models can be realized through frequency transformations.

In order to dimension waveguide filters, the standard lowpass lumped element model is transformed by using immittance inverters. The inverter model is composed by a cascade of inverters separated by lamped elements. Each inverter represents coupling elements in filter structures, while lamped elements represent the propagating waveguides. In the next chapter, RF requirements will be introduced including a detail information and limitation of the current technologies.

2.6. References

[2-1] W. P. Mason and R. A. Sykes, "The use of coaxial and balanced transmission lines in filter and wide band transformers for high radio frequencies", *Bell Syst. Tech. J.*, vol. 16, pp. 275-302, 1937.

[2-2] G. L. Matthaei, L. Young, and E. M.T. Jones, *Microwave Filters, Impedance-Matching Networks and coupling Structures*, New York: McGraw-Hill Book Co., 1964

[2-3] S.B. Cohn, "Direct- Coupled- Resonator Filters", Proceedings of the IRE, vol. 45, pp. 187-196, February 1957.

[2-4] R. Levy, "Theory of Direct Coupled Cavity Filters", IEEE Transaction on Microwave Theory and Techniques vol. MTT-11, N0. 6, pp. 340-348, June 1967

[2-5] G. Conciauro, M. Guglielmi, R. Sorrentino, *Advanced Modal Analysis,* New York: John Wiley & Sons, LTD 1999

Chapter 3 – Filter requirements and current design limitations

The new MAP science mission will bring results into focus with an elevated level of detail and accuracy, detecting the celestial cosmic background with a higher precision than the previous mission. The intent is to replace the critical system that has previously caused the most losses. Part of this process is the introduction of new Microwave components, which exhibit lower losses in comparison to the classic NASA technology that makes use of large, very lossy optical components. The novel instrument shall exhibit low insertion loss within the specified bandwidths and high rejection in the out-of-band frequency range (Fig. 3-2). This Microwave waveguide structure replaces optical elements, improving the accuracy of the measurement system and drastically reducing the system losses. In this chapter, a general description of the ending part of the instrument will be described. RF specs will be also discussed together with the related problems.

3.1. Science instrument front-end

As previously mentioned, the novel science instrument will be composed by microwave components that replace standard NASA technology.

The instrument's front-end will be composed of a radiating waveguide array, which will behave as an antenna. The array will be composed of one thousand circular waveguides in parallel, composing the antenna beam. Each circular waveguide shall represent a "pixel" of the celestial microwave background. The circular waveguides will be close to each other, exhibiting small diameters in the millimeter range. Fig. 3-1 depicts an example of the science instrument front-end array. As mentioned, each circular waveguide will behave as an antenna receiving the electromagnetic field. Beyond those "waveguide circles", the filtering mechanism will take place.

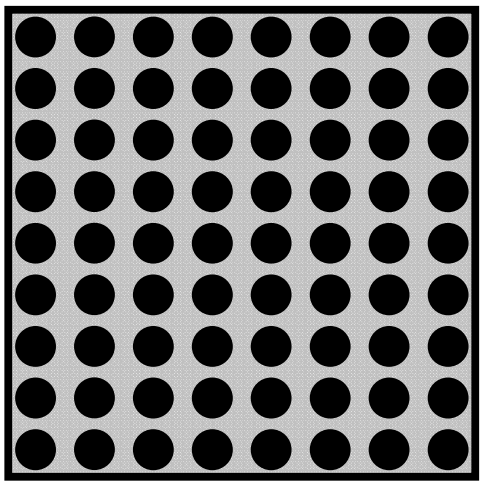

Fig. 3-1: Science instrument front end array (example).

In fact, filters will be positioned behind each circular waveguide. As a consequence, the number of filters necessary for the instrument will be high. The intent of the instrument will be to measure the polarization of the cosmic background and to guarantee high rejection in a wide frequency range.

3.2. RF requirements

The filtering mechanism of the instrument is located beyond each receiving circular waveguide. The entire instrument will reject from 60 GHz until 700GHz, which is the physical limit for superconducting materials. After 700 GHz, superconductors stop behaving as superconductors and this is out of the region of interest. No single component is known to be able to reject from 60 GHz until 700 GHz, however it is believed that the result could be achieved by a “joined effort”. In other words, the hope is to use several different elements in cascade to achieve the result.

NASA has already developed part of the instrument, realizing for the first time microstrip filters rejecting up to 8.5 harmonic [3-7], [3-8] (results proved by measurements). A positive outcome of the new, more efficient behavior of the filter component is that the additional components are resultantly simpler to design.

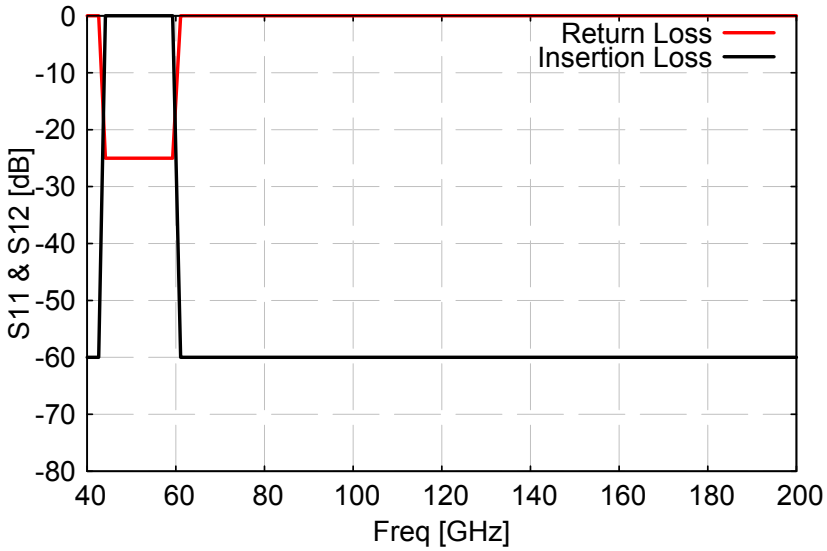

Fig. 3-2: S-parameters goal functions

The additional components will be waveguide filters immediately behind the circular waveguides, in front of aforementioned filtering mechanism. This work has the aim of presenting the *missing* part, the additional waveguide filters. The latest investigations and results of this *missing* part will be presented in this work.

The microwave shall exhibit the following RF specifications:

- Fractional bandwidth ~ 30%
- Higher transmitted frequency $\geq$ 60 GHz
- In-band Return Loss $\geq$ 20 dB
- In-band insertion loss <1 dB
- Out-of-band insertion loss $\geq$ 60 dB between 63 and 200 GHz
- The filter should Preserve both polarization states

- Power handling None
- Isolation of the two polarization verify

The requirements can be visualised with an S-parameter goal function (mask) as in Fig. 3-2.

3.3. Polarization states issue

In order to preserve the polarization states and guarantee the extreme rejection requirements, two different approaches can be followed.

1. Make use an orthomode transducer (OMT)
2. Use a single filter structure with 4-fold symmetry

The first approach is conventional and requires separating the polarization in two different channels and consequently filtering the two signals [3-1], [3-2], [3-3], [3-4]. After the separation, the two polarizations can be treated using a standard waveguide filters; e.g., rectangular waveguide filters. However, rectangular waveguide filters cannot guarantee such extreme rejection by themselves, and waffle iron filters, following the filter in cascade, would be necessary. As is known, the waffle iron filter has the quality of *cleaning* spurious modes until 4^{th} harmonic. This approach is very efficient in terms of rejection, however it introduces complexity. In fact, two waveguide filters would be necessary for each *circular pixel* of

Fig. 3-1. If the radiating elements of Fig. 3-1 are a thousand, than two thousand filters would be required in conjunction with waffle iron filters. Moreover, positioning OMTs behind the radiating arrays is difficult because of restraints in physical dimensions.

The second approach, the use of a single filter structure with 4-fold symmetry, seems to be better in terms of space and components number saving. This approach has been investigated and will be discussed in this work.

3.4. Square and circular waveguide structure

Polarization requirements need the filter cross-section to exhibit four-fold symmetry, which is able to preserve the polarization states of the electromagnetic field. Standard waveguides that exhibit four-fold symmetry are circular and square waveguides [3-5]. However, filters realized with this technology offer poor out-of-band rejections [3-6] because of the intrinsic topology of the structures. In fact, many modes propagate in the frequency range between 40 and 200 GHz, making the attainment of acceptable rejection impossible. Recently, NASA/GSFC has spent much time improving the rejection up to frequency around 6.1 times the centre frequency of the filter [3-7], [3-8]. Unfortunately, these filters are not developed in waveguide technology.

Using simple and well-known formulas, it is possible to analytically calculate the existing modes into rectangular (and square). In particular,

the cut-off frequencies of the propagating modes can be calculated using the following formula:

$$f_c = \frac{c}{2\pi}\sqrt{\left(\frac{m}{a}\pi\right)^2 + \left(\frac{n}{b}\pi\right)^2}$$

where, *c* is speed of light, *m*, *n* are the mode indexes and *a*, *b* are the cross-section dimensions. When *b* is equal *a* (square case), TM11 (and TE11) become the second order mode appearing in the waveguide structure. For many practical applications in rectangular waveguide, TE20 and TE30 mode generally define the limit of the rejection frequency range being the second and the third higher order modes of the waveguide.

For the case under consideration in this work, if we calculate propagating mode in the square waveguide 4.775x4.775 mm we can calculate the following propagating modes untill 200 GHz:: TE01, TE10, TM11, TE11, TE02, TE20, TM12, TE12, TM21, TE21, TM22, TE22, TE03, TM13, TE13, TM31, TE31, TM23, TE23, TM32, TE32, TE04, TE40, TM14, TE14, TM41, TE41, TM33, TE33, TM24, TE24, TM42, TE42, TE05, TM34, TE34, TM43, TE43, TE50, TM15, TE15, TM51, TE51, TM25, TE25, TM52, TE52, TM44, TE44, TM35, TE35, TM53, TE53, TE06, TE60, TM16, TE16, TM61, TE61, TM26, TE26, TM62, TE62. Fig. 3-3 depics all the propagating modes in the square waveguide 4.775x4.775 mm until 200GHz.

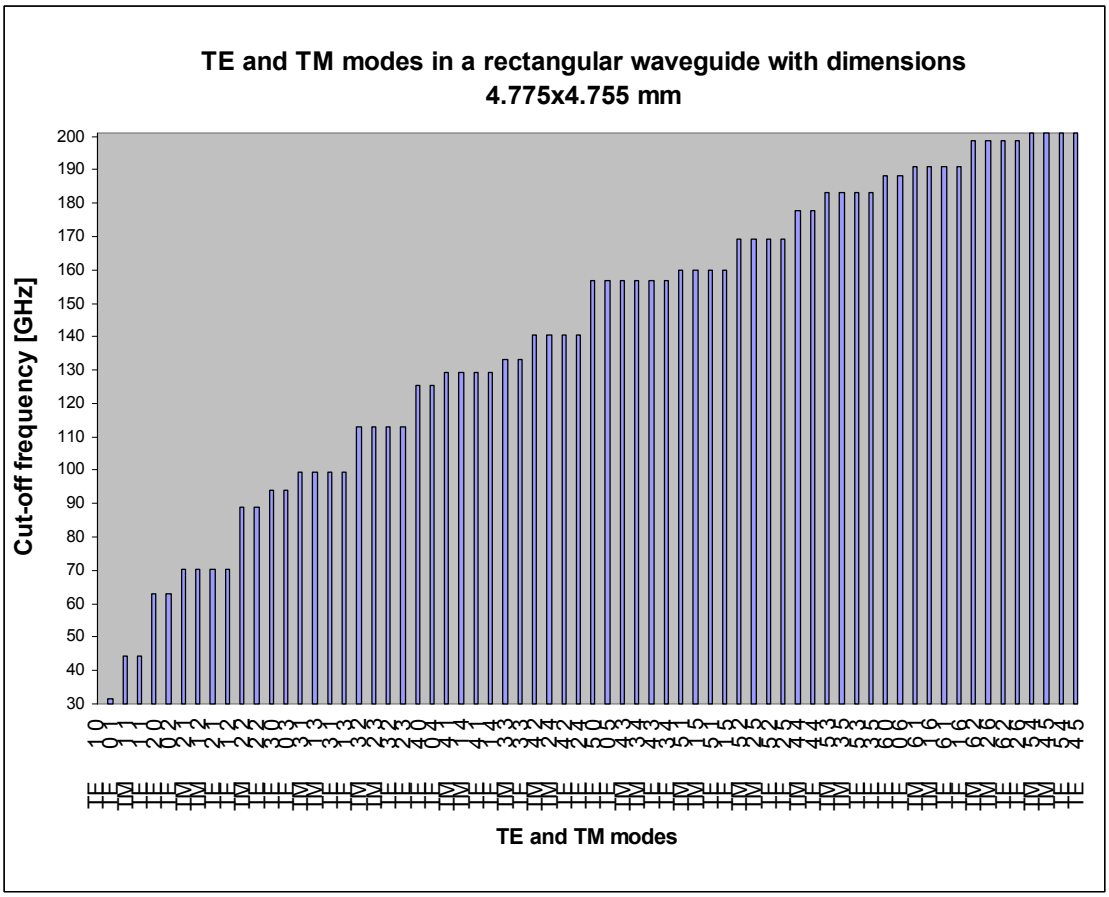

Fig. 3-3: List of TE and TM modes in a square rectangular waveguide of dimensions 4.775x4.775 mm. Modes are sorted for cut-off frequency and the until 200GHz.

Consider the following case as a practical example of the effect of higher order modes on the filter rejection:

- Waveguide type (rectangular) WR15
- Filter order 2
- Return loss in band 25 dB
- Length of each iris 0.5 mm
- Center Frequency 50 GHz
- Bandwidth 600 MHz

Following the dimensional synthesis procedures described in [3-9] for inductive iris filters, the following dimensions can be found:

- Resonator lengths 3.211, and 3.211 mm
- Iris widths 2.207, 1.5, and 2.207 mm

It is worthy to note that the filter dimensions are completely symmetric in respect to the center of the structure. Using mode-matching code Fig. 3-4 is generated, where only the insertion loss is plotted between 40 and 200 GHz.

The use of Fig. 3-4 is only qualitative, in fact after 88 GHz the structure is no longer monomode and what is plotted until 200 GHz cannot be trusted. In fact, higher order modes start propagating and their impact is evident on the insertion loss. In other words, part of the energy of the fundamental mode is distributed to other modes that start propagating at their cut-off frequencies. This well known phenomenon translates into the difficulty of having ideal rejection response.

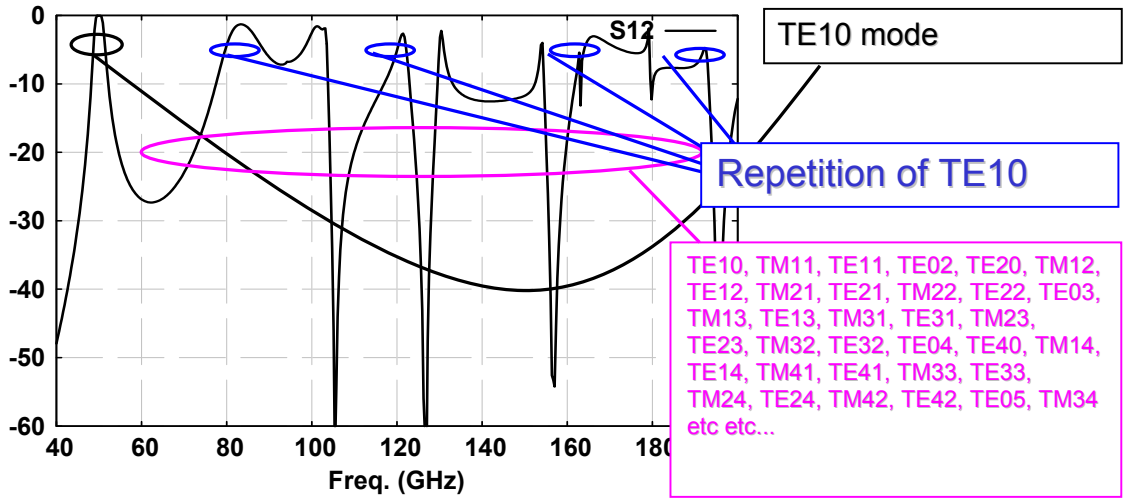

Fig. 3-4: Insertion loss response between 40 and 200 GHz of a 2 pole Chebyscheff filter using standard rectangular. TE101 mode and its repetitions (TE102, TE103, and TE105) are in evidence. The higher order modes are also indicated.

If the effect of higher mode is so strong in rectangular waveguides, it becomes even worse in circular or square waveguides. In fact, the bigger dimensions (4.775x4.775 mm) introduce more modes in the structure. In conclusion, the repetition of the fundamental mode and the higher order modes forbid the filter to achieve extreme rejection response as required by the specifications.

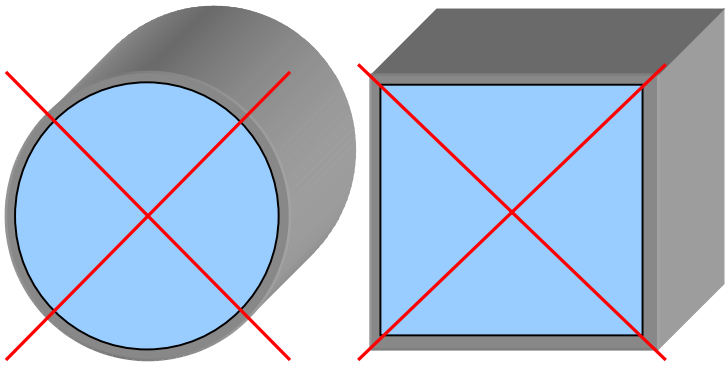

Fig. 3-5: Circular and square waveguides cannot be used in this filter design.

Again, as both explained and presented with the figures above, the high number of propagating modes translates into the total impossibility of having acceptable rejection in the band of interest through the use of square or circular waveguides (see Fig. 3-5). As a result of these findings, this work will now continue with an investigation into a more appropriate quadruple ridge waveguide filter that allows for acceptable rejection.

3.5. Summary

Chapter 3 briefly introduced the front-end of the science instrument, the RF requirements for the filter, and the issue of handling both polarization states of the electromagnetic field. This chapter also discussed the limitations in current filter designs, namely the problems of higher order modes and rejection in circular and square waveguide structures.

3.6. References

[3-1] A.M. Boifot, E. Lier, T. Schaug-Pettersen, “Simple and broadband orthomode transducer” IEE proceedings, Vol. 137, Pt, H, No. ^,December 1990.

[3-2] G. Chottopadhyay, B. Philhour, J. Carlstrom, S. Church, A. Lange, and J. Zmuidzinas, “A 96-GHz Ortho-Mode Transduced for the Polatron”, IEEE Microwave and Guided Wave Letters Vol. 8, No. 12 December 1998

[3-3] N. Yoneda, M. Miyazaki, T. Noguchi, “A 90GHz –Band Monoblock Type Waveguide Orthomode Transducer”, IEEE MTT-S Digest 1999

[3-4] M.P. Natarov, L.A. Rud, V.I. Tkachenko, “Orthomode Transducer for mm-wave range”, MSMW’04 Symposium Proceedings. Kharkov, Ucraine, June 21-26, 2004

[3-5] Chung-Li Ren, and Han-Chiu Wang “H01 circular waveguide low-pass filter for millimeter wave transmission system”

[3-6] Smain Amari, and Jens Bornemann, “Design of polarization-preserving circular waveguide filters with attenuation poles”, Microwave and optical technology letters Vol.31, No.5, December 5 2001

[3-7] K. U-yen, E. J. Wollack, T. Doiron, J. Papapolymerou, and J. Laskar, “The Design of a Compact, Wide Spurious-free Bandwidth Bandpass Filter Using Stepped Impedance Resonators,” accepted to the IEEE 8th European Microwave Conf., Paris, France, October, 2005.

[3-8] K. U-yen, E. J. Wollack, T. Doiron, J. Papapolymerou, and J. Laskar, “A Bandpass Filter Design With Extended Rejection Bandwidth Using Double Split-end Stepped Impedance Resonators, “ to be submitted to IEEE Microwave Theory Tech., July 2006.

[3-9] Felice Maria Vanin, Dietmar Schmitt, Ralph Levy, “Dimensional Synthesis for Wideband Wave Guide Filters”, IEEE International Microwave Symposium, Fort Worth, Texas (US), June 2003.

Chapter 4 – Quadruple ridge waveguide filter

As this work has explained the impossibility of using standard waveguide components for the proposed design, the properties and capabilities of a different waveguide cross-section will be investigated. Therefore, this work proposes the use of a quadruple ridge waveguide cross section, which is fundamentally different from a square structure without ridges, shown in Fig. 4-1. The structure is square and exhibits four ridges that enter deep inside the structure from the center of each face. This cross section is known in literature [4-1], but to my knowledge no practical filter design has been realized with this cross-section.

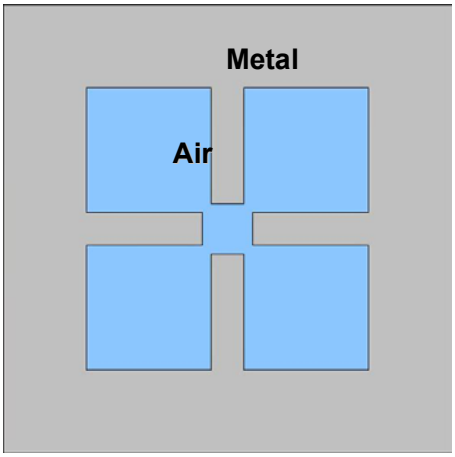

Fig. 4-1: Quadruple ridge cross-section

As known from electromagnetic theory, the cross section defines the propagating modes inside the filter structure. When the dimensions of the cross section are fixed, the cut-off frequencies of the fundamental mode and the higher order modes are defined. The reason for the use of this cross section is for the shifting higher in frequency the appearance of second order modes. In fact, it is known [4-2] that ridge waveguide structures have the property of improving the separation between fundamental mode and second order modes. In other words, the introduction of the ridges within the waveguide results in the shifting of fundamental modes down in frequency, while shifting second order modes higher in frequency. Thus, the appropriate cross-section design fixes the propagating modes in the structure. As already mentioned in the RF filter specs, the rejection must be less than 60 dB between 60 and 200 GHz. This translates in designing the cross-section in order to have the second propagating mode at 200GHz.

4.1. Polarization issue

It is evident that also in this case, the four-fold symmetry preserves the dual polarization states of the electromagnetic field. For example, if the cross section is excited with a linearly polarized field (vertical in both directions) the electric field lines and field intensity will occur in the quadruple waveguide structure as is shown in Fig. 4-2 and Fig. 4-3 (one

quarter of the structure is shown). The field lines are stronger on the edge of the ridges where the minimum distance within the structure occurs.

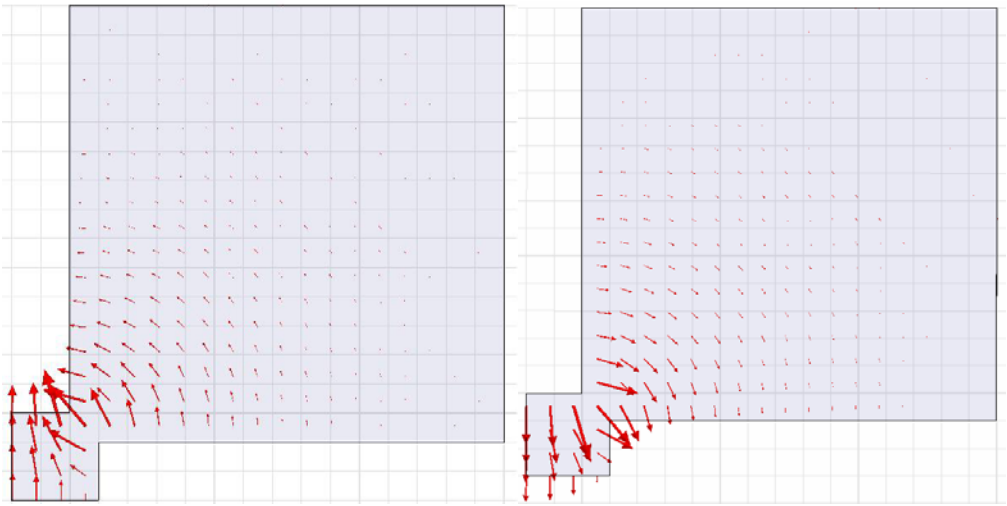

(a) *(b)*

Fig. 4-2: E-Field's lines. (a) if excitation is linearly vertically polarized (vector pointing up). (b) if excitation is linearly vertically polarized (vector pointing down)

On the other hand, if the excitation is horizontal linearly polarized, the field's lines and field's intensity will occur in the structure as is shown in Fig. 4-4 and Fig. 4-5 (one quarter of the structure is shown).

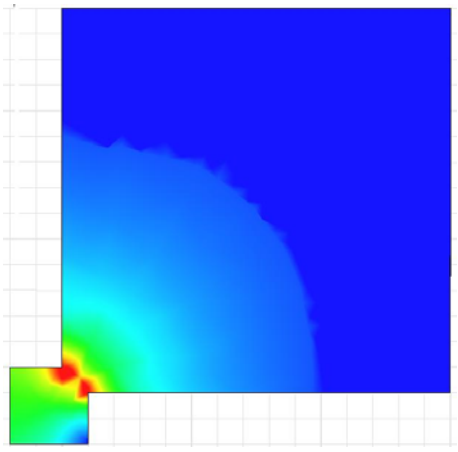

Fig. 4-3: E- Field's intensity first polarization

It can be noted that both the field's lines and the field's intensity maintain symmetry as well as the waveguide cross-section.

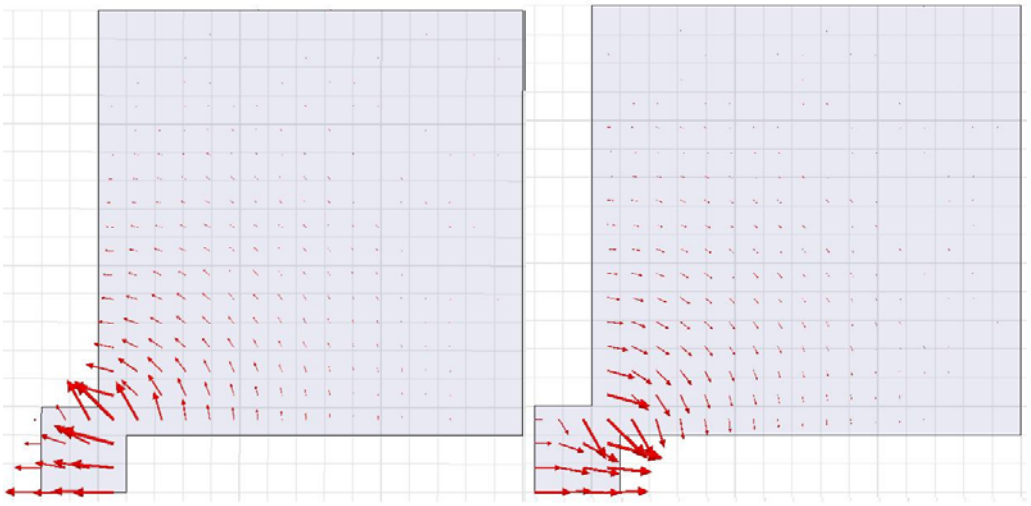

(a) *(b)*

Fig. 4-4: E-Field's lines. (a) if excitation is linearly horizontally polarized (vector pointing left). (b) if excitation is linearly horizontally polarized (vector pointing right)

Therefore, this cross-section appears ideal for this application. In fact, the two field state polarizations can be treated at the same time, shifting the cut-off frequency of the second propagating mode higher.

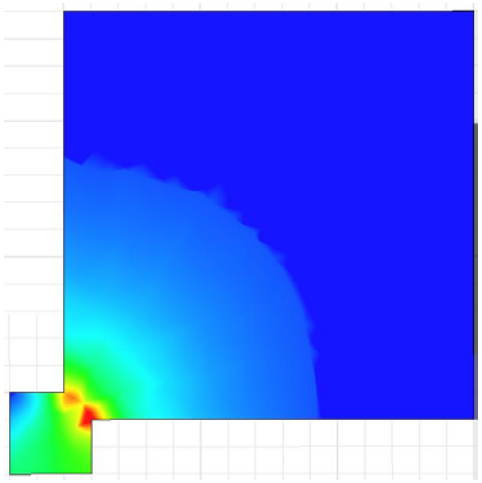

Fig. 4-5: E-Field's intensity second polarization

For orthogonality and symmetry the two polarizations are not coupled. For the particular design under consideration, the cross-section shall be designed in order to have the fundamental mode starting at 40 GHz and the second propagating mode at 200 GHz.

4.2. Design procedure, cross section design and coupling behavior

In order to achieve the filter design with the given RF specs, the following steps shall be followed:

1. Realize the network model following the steps in chapter 2
2. Design appropriately the waveguide cross-section according to RF specs
3. Calculate initial dimensions following known dimensional synthesis techniques as in [4-3]
4. Cascade appropriately quadruple ridge waveguide sections with empty waveguides
5. Optimize the structure if necessary

According to fullwave simulations performed using two different mode matching codes; the geometry shown in Fig. 4-6 has the cut-off frequency of the fundamental mode at 39.5 GHz and the second propagating mode at 200 GHz. This result is the first important step in the design; in fact, the frequency range between 60 and 200 GHz is entirely occupied only by the fundamental mode.

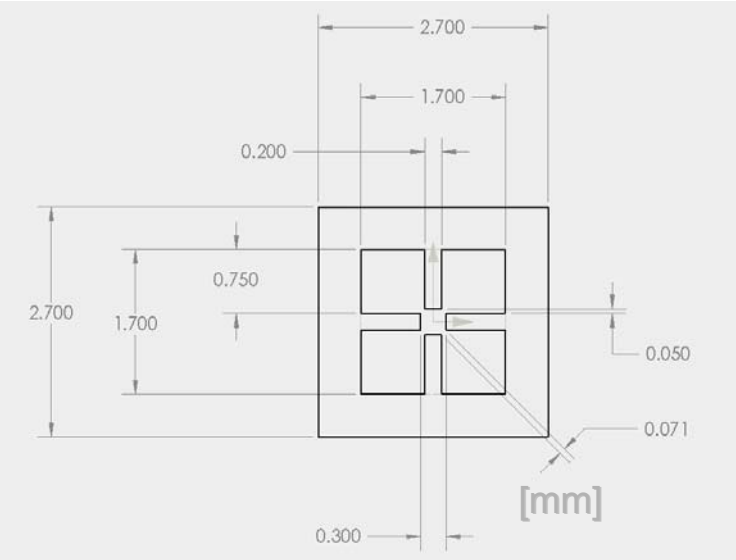

Fig. 4-6: Quadruple ridge cross-section's dimensions [mm]

As expected, the width and height of the quadruple cross-section are three times smaller than the standard square waveguide WR 19, while they both exhibit the same operative frequency range.

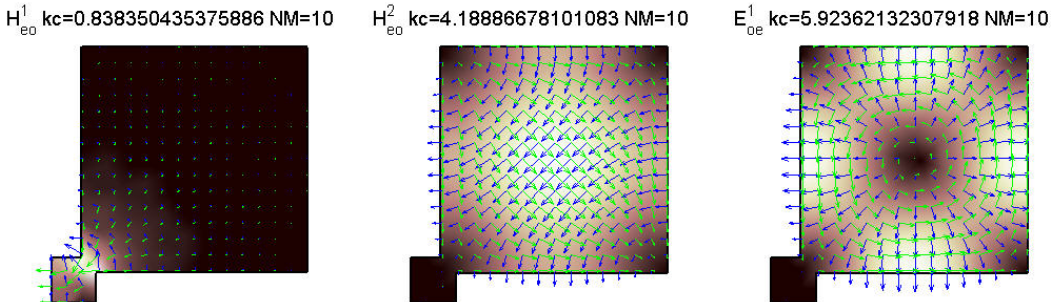

Fig. 4-7: First three propagating modes is the quadruple cross-section. The first mode appears at 39.5 GHz, the others two at 200 GHz. Only one quarter of the cross-section is shown.

Fig. 4-7 shows the field's intensity, the field's lines and propagation constant of the first three propagating modes; one quarter of the cross-section only is shown. The fundamental mode is concentrated in the vicinity of the ridges and it exhibits no field in the corners of the housing.

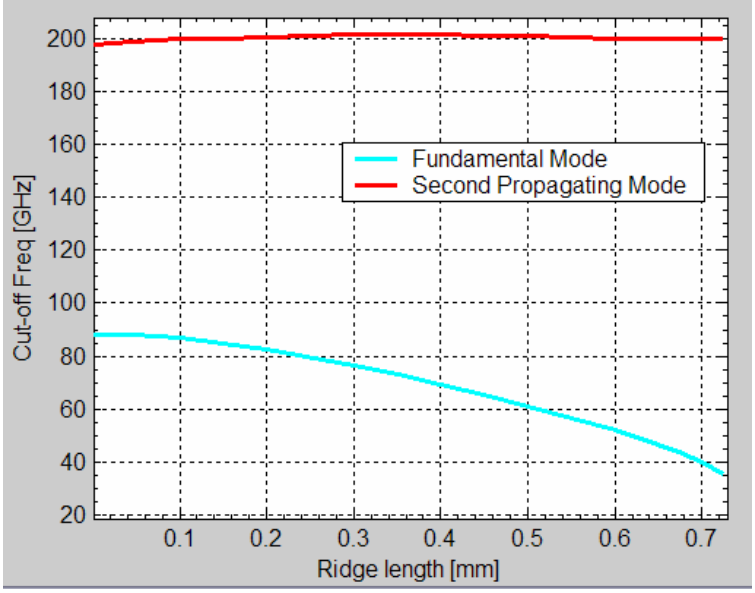

Fig. 4-8: Cut-off frequency of the fundamental mode and the second propagating versus ridge length in the quadruple ridge cross section. The width and height have been fixed to 1.7 mm and the ridge width to 0.2 mm.

On the other hand, the other two modes are mainly concentrated in the four regions, separated by the ridges. As mentioned, the first mode appears at 39.8 GHz, while the other two after 200 GHz. Fig. 4-8 shows the behaviors of the cut-off frequency of the fundamental and second propagating modes as a function of the ridge length. The cut-off frequency of the fundamental mode varies in frequency from 88GHz to 35 GHz with ridges lengths that vary from 0 to 0.74 mm. On the other hand, it can be noted that the cut-off frequency of the second propagating mode is approximately constant to 200 GHz. If two quadruple cross sections (dimension given in Fig. 4-6) are separated by an evanescent square waveguide section, impedance inverter values can be calculated as a function of the coupling section length. Fig. 4-9 depicts the inverter behavior as a function of the coupling length solved for 51.6 GHz;

however, this behavior is the same for other frequency points. It can be noted that inverter values bigger that 0.7 cannot be achieved with practical length. In fact, the coupling section would be smaller than 0.06 mm, which evidently is a dimension too small to be realized. Inverter values bigger than 0.7 might be typical of wide band filters with fractional bandwidth of approximately 30%.

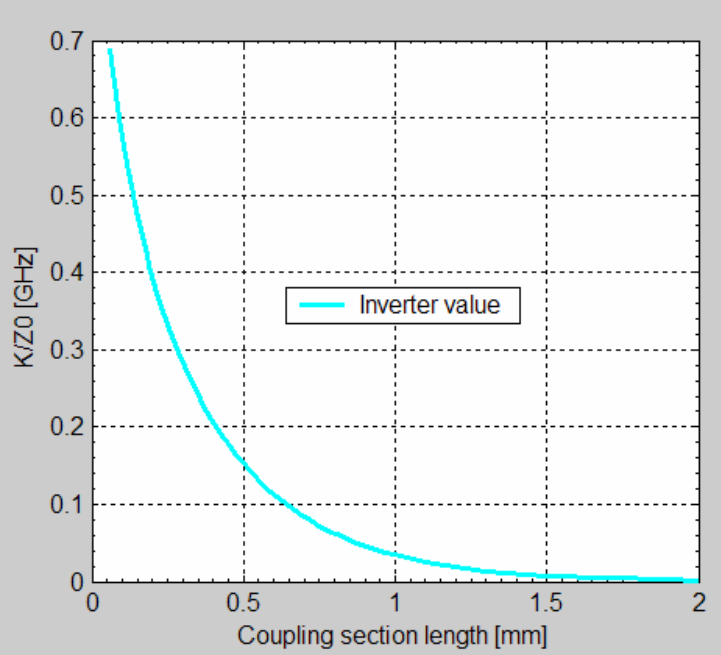

Fig. 4-9: Inverter behaviors versus coupling section length in millimeter value. The minimum length considered in the plot is 0.06 mm. The inverters are solved for 51.6 GHz.

After having determined the cross section of the waveguide, several filter designs have been realized following the above mentioned design procedure. In this work, three different filter designs are considered and used to present the properties of this novel structure.

4.3. 2-pole filter design

Using the cross-section shown in Fig. 4-6, a 2-pole filter has been realized with the following RF specs:

- 2-pole filter design
  - center frequency 49.775 GHz
  - In band return loss 25 dB
  - Fractional bandwidth 5.8%

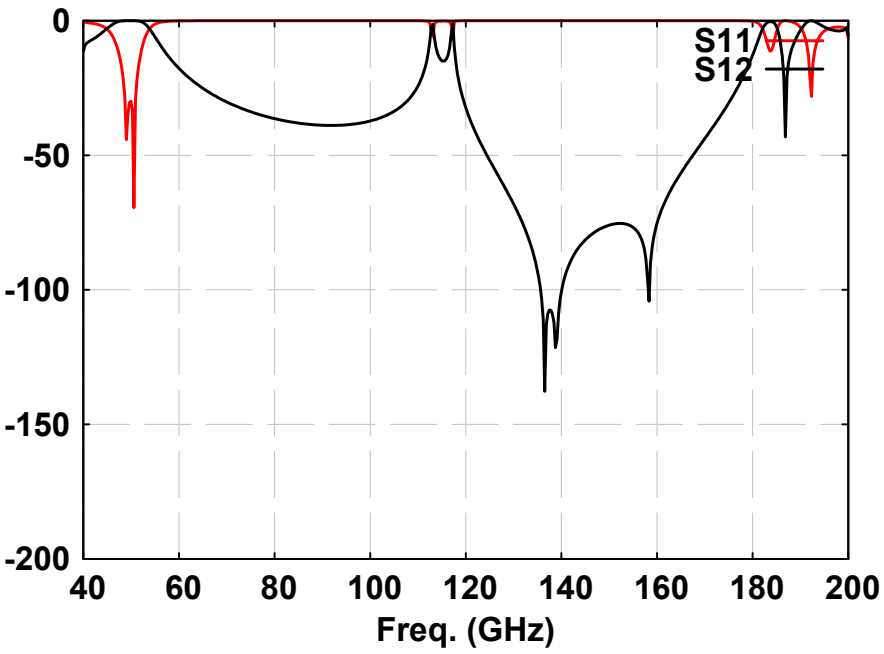

Fig. 4-10: 2 pole filter response.

Fig. 4-10 shows the S-parameter response; the plot has been generated using mode-matching code and the S-parameters are normalized to the wave impedance of the quadruple ridge waveguide. The filter structure is completely symmetric and the mechanical dimensions are given in millimeter in Fig. 4-11.

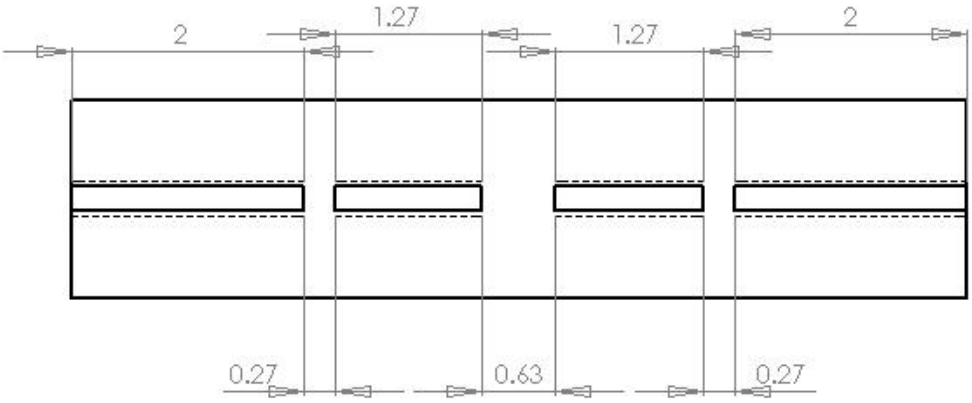

Fig. 4-11: Technical drawing, longitudinal view of the 2-pole filter (dimensions in mm).

4.4. 6-pole filter design

Using the cross-section shown in Fig. 4-6, a 6-pole filter has been realized with the following RF specs:

- 6-pole filter
    - center frequency 51.9 GHz
    - In band return loss 25 dB
    - Fractional bandwidth 27%

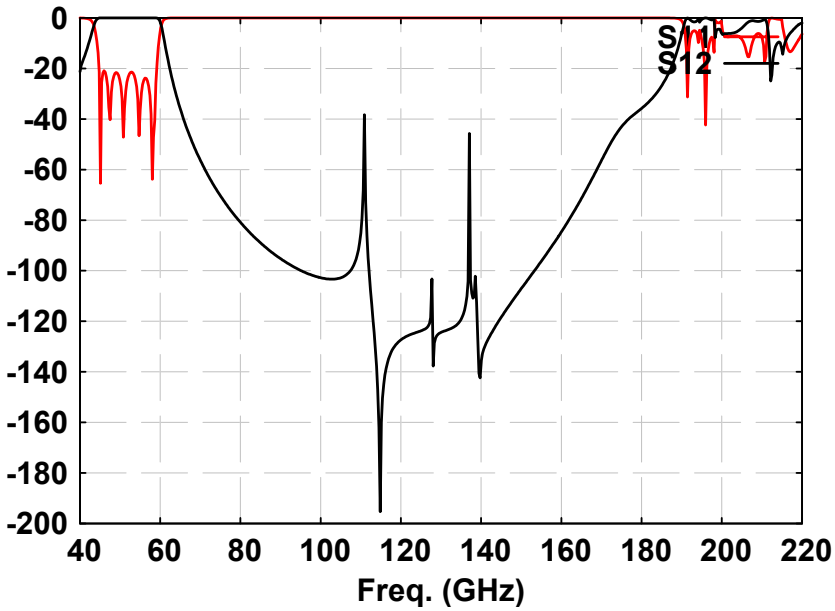

Fig. 4-12: 6 pole filter response.

Fig. 4-12 shows the S-parameter response; the plot has been generated using mode-matching code and the S-parameters are normalized to the wave impedance of the quadruple ridge waveguide. The filter structure is completely symmetric and the mechanical dimensions are given in millimeter in Fig. 4-15. Fig. 4-15 shows that the first input coupling length is very small (just 0.078 mm) and it is too small to be realized with the actual technology. This length is very important since it determines the in-band return loss. A solution to overcome the problem of the small input coupling will be discussed later in this work.

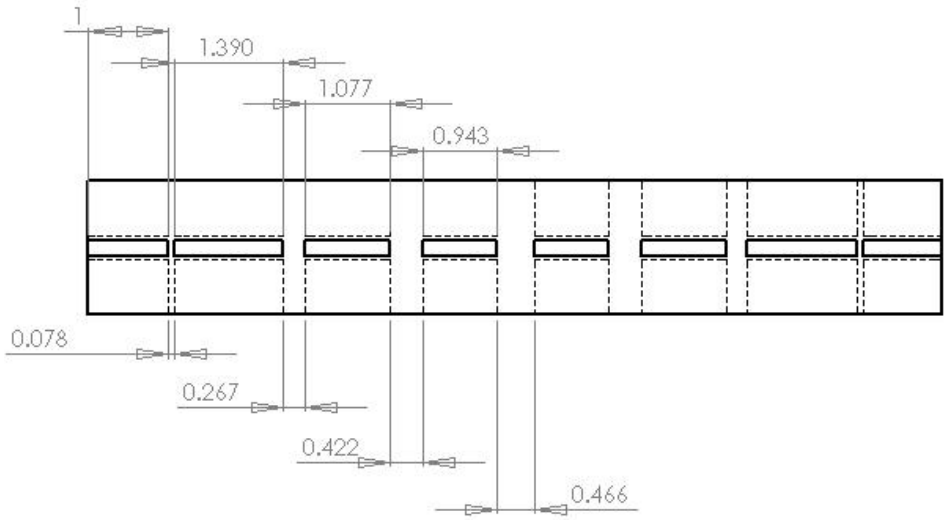

Fig. 4-13: Technical drawing, longitudinal view of the 6-pole filter (dimensions in mm).

4.5. 7-pole filter design

Using the cross-section shown in Fig. 4-6, a 7-pole filter has been realized with the following RF specs:

- 7-pole filter
    - center frequency 51.6 GHz
    - In band return loss 20 dB
    - Fractional bandwidth 30%

Fig. 4-14 depicts the responses the 7-pole filter. This plot has been generated using mode matching code, and that the S-parameters are normalized on the wave-impedance of the quadruple ridge waveguide.

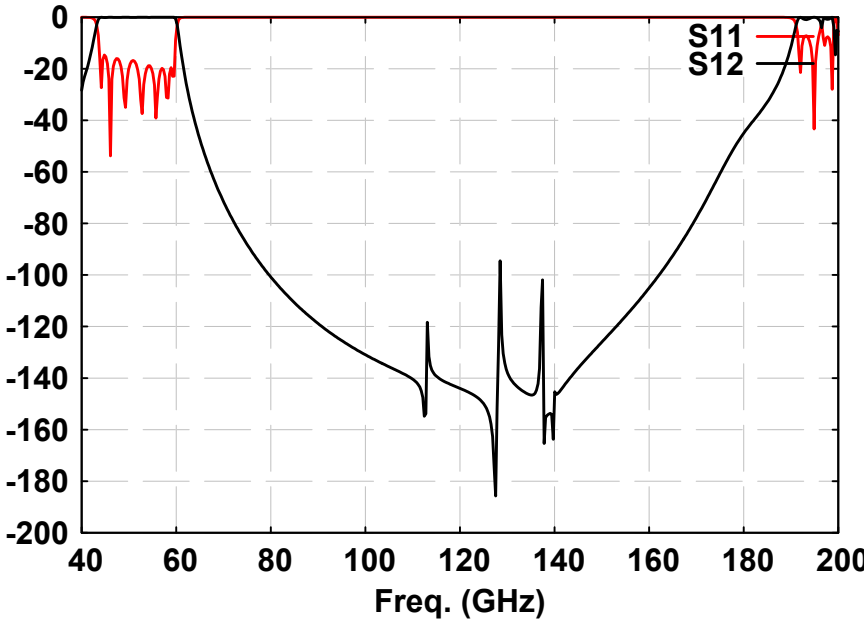

Fig. 4-14: 7 pole filter response.

From the fullwave simulations on the three filters the following considerations are valid:

1) At 50 GHz, the resonant mode TE101 creates the filter response.
2) Around 110 GHZ, one “spike” appears for each resonator. The repetition of the fundamental mode TE102 appears.
3) Increasing the filter order, the repetition of the fundamental mode TE102 *tends to be suppressed*.
4) The spikes are function of the bandwidth of the filter and its resonator length.
5) Increasing the order of the filter, zero of transmissions are generated.

6) The second propagating mode appears as foreseen from the cross section design.
7) Repetition of the fundamental mode can be suppressed increasing the filter order.
8) The second propagating mode (TE301) starts at 200GHz.

As shown in the simulations, the repetition of the fundamental mode (mode TE102) is suppressed by increasing the number of poles in the structure. It should be noted that this result of “killing” the repetition of the fundamental mode by increasing the filter order is a property of this waveguide structure and it is not happening in standard waveguide structures.

The seven-pole filter complies with the rejection requirements, adequately suppressing the repetition of the fundamental mode occurring at 110 GHz, as shown in Fig. 4-14. It can be seen that rejection is quite good until 200 GHz, where the second mode appears as predicted.

Fig. 4-15 and Fig. 4-16 show 3D-drawings of the filter. Sections of the structure are shown offering view of the inside of the filter.

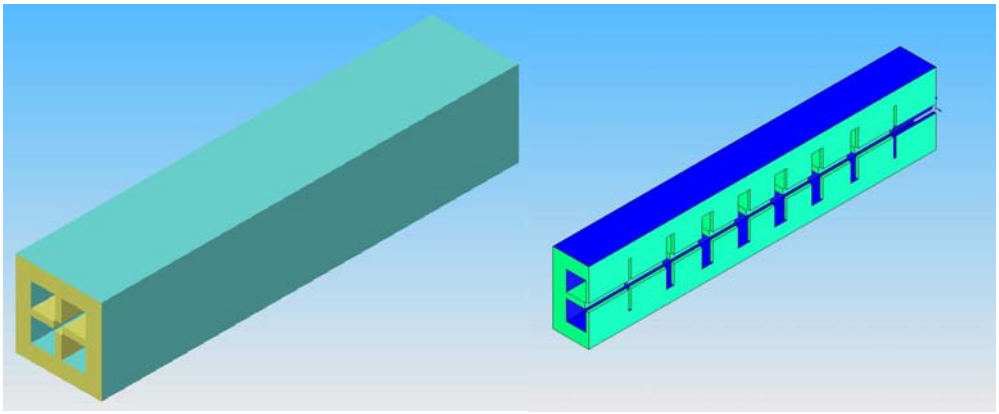

(a). *(b)*

Fig. 4-15: 3D drawings of the filter structure. (a) Entire structure, (b) longitudinal section.

In Fig. 4-15 and Fig. 4-16, the propagating waveguide sections are evidently separated by the evanescent sections. The propagating waveguides, which are shown in Fig. 4-16 from 1 to 7, behave as resonators, while the first and the last waveguides represent the input and output waveguides of the filter. The evanescent coupling sections are in evidence as well in Fig. 4-16.

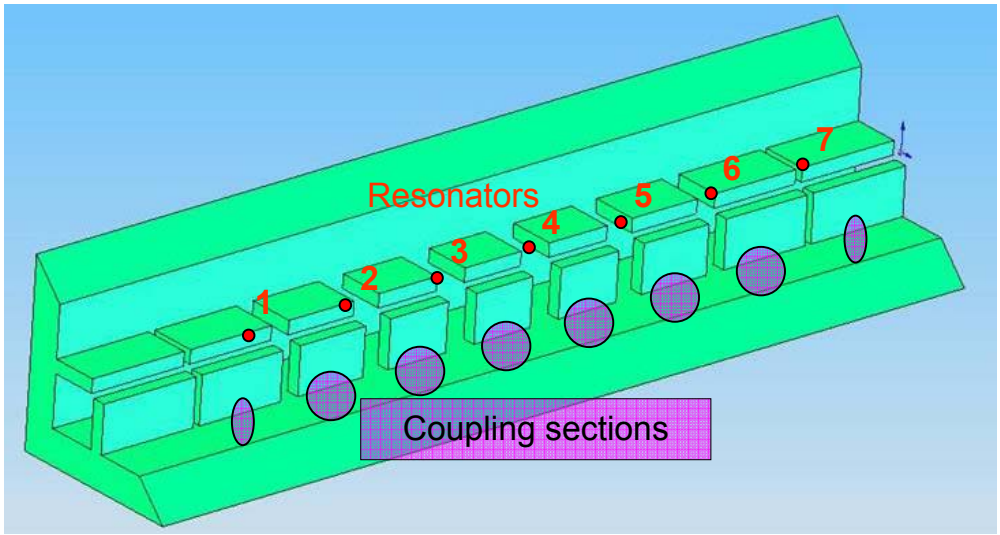

Fig. 4-16: 3D-drawings of the filter structure. Longitudinal section with cut plane at 45 degree angle. Resonators and coupling elements are in evidence.

In band S-parameter response is given in Fig. 4-17.

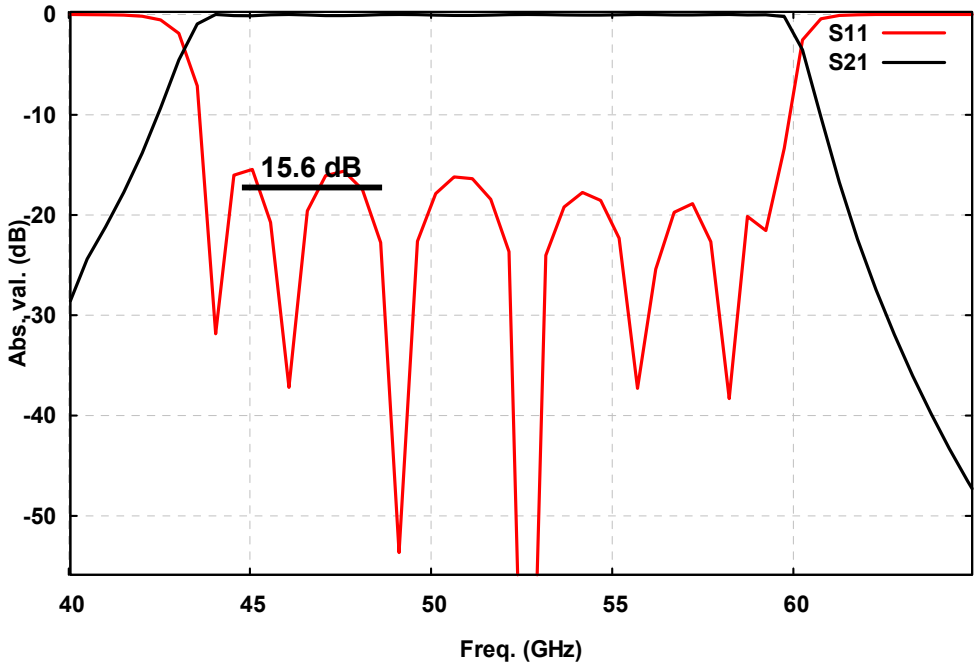

Fig. 4-17: In-band response.

Bandwidth goes from 43.7 until 59.5 GHz, the center frequency is 51.6 GHz, and the fractional bandwidth is approximately 30%.

The filter designs are obtained by adjusting opportunely the length of each section (quadruple ridge and evanescent section). In particular, the input coupling determines the in-band return loss, which is better than 15 dB in the whole frequency range. In order to have better return loss, the first evanescent section should be smaller in length than 0.1mm. However, this 0.1 mm is a fixed dimension due to physical machinability limits in NASA/Goddard.

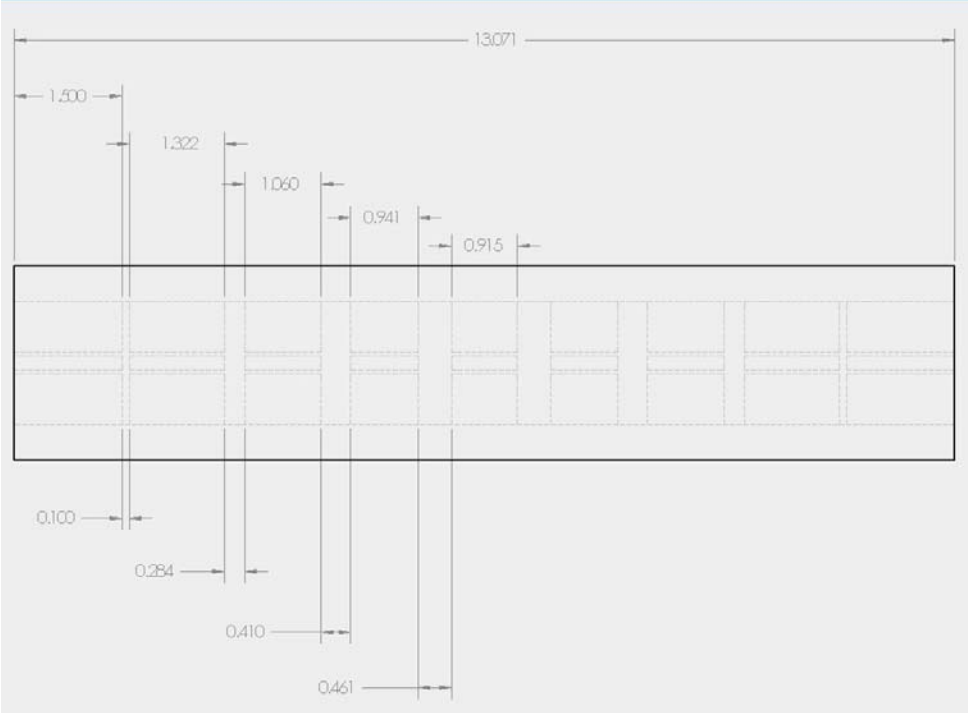

Fig. 4-18: Technical drawing, longitudinal view of the 7-pole filter (dimensions in mm).

4.6. Higher order mode suppression

In order to understand the phenomena of higher order mode suppression, it is necessary to study the elementary contribution of each evanescent section. In fact, as it will be known, each section introduces a zero of transmission in the frequency-range of interest.

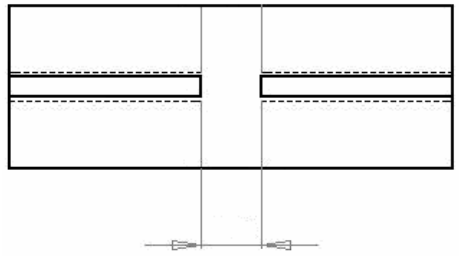

Fig. 4-19: Two quadruple ridge sections separated by an evanescent section.

By fullwave simulating a structure composed of two quadruple ridge sections (input-output) separated by an evanescent section as shown in Fig. 4-19, an interesting result can be found. Fig. 4-20 depicts the S-parameter response of each evanescent section. It can be noted that a transmission zero is introduced in the out-of-band frequency range.

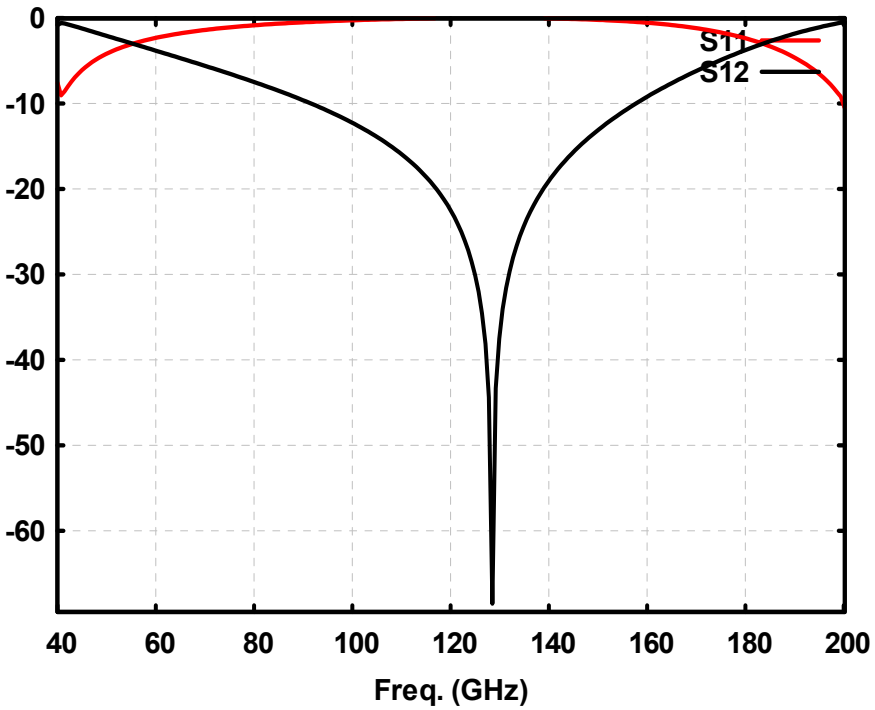

Fig. 4-20: S-parameter response of two quadruple ridge sections separated by an evanescent section.

The position of the transmission zero depends only from the length of the evanescent section. Therefore, the zero changes its position in frequency according to the length of the evanescent section. The appearance of the transmission zero is likely due to the abrupt change of impedance between the quadruple ridge section and the empty square ridge section. This result is consistent with what is observed in the filter design. For each

evanescent section, a zero of transmission is created. Therefore, these zeros are the basic mechanism for the higher order mode suppression. The higher the filter order, the higher the number of zeros, which translates into stronger suppression. In conclusion, the zeros of transmission, due to the evanescent sections, are the cause of the suppression of the higher order mode.

This conclusion is now validated with a network model representation. A waveguide filter can be represented by the model (see Fig. 2-8), which uses inverters for the characterization of Chebyscheff responses. However, these inverters are ideal lumped elements and do not exhibit any frequency dependence. An ideal inverter behavior translates into a constant frequency response. In other words, if the coupling section of Fig. 4-19 had been ideal, the frequency response of Fig. 4-20 would have been flat from 40 until 200 GHz with a specific Return and Insertion loss value [4-6]. This means that the network model is far from ideal, though it is still a good approximation in the vicinity of the bandpass filter response i.e. between 40 and 60 GHz.

A concept that it is well known but often taken for granted *is the process of converting any lossless passive reciprocal two-port into an impedance inverter* [4-5].

In this case, Fig. 4-19 represents a two-port element defined by its frequency dependent transfer matrix obtained from fullwave analysis [4-6]:

$$A_{Fullwave} = \begin{pmatrix} A(\omega) & jB(\omega) \\ jC(\omega) & D(\omega) \end{pmatrix}$$

Now, by choosing two reference planes P1 and P2 at electrical distance $\phi 1$ and $\phi 2$ from the respective ports it is possible to convert the two-port into an impedance inverter [4-5]. However, the two port element will behave as an inverter at only one frequency point. This is because of the intrinsic frequency dependence of the coupling section that should be taken into account [4-6].

Now, on these bases it is possible to create a network model that takes into account the frequency behavior of the coupling sections. Each inverter of Fig. 2-8 can be replaced by $A_{Fullwave}$ matrix that takes into account the frequency dependence of the coupling section, *including the transmission zero* noted in Fig. 4-20. A more accurate network model can be achieved by taking into account the frequency dependent couplings and taking into account the transmission zeros Fig. 4-23.

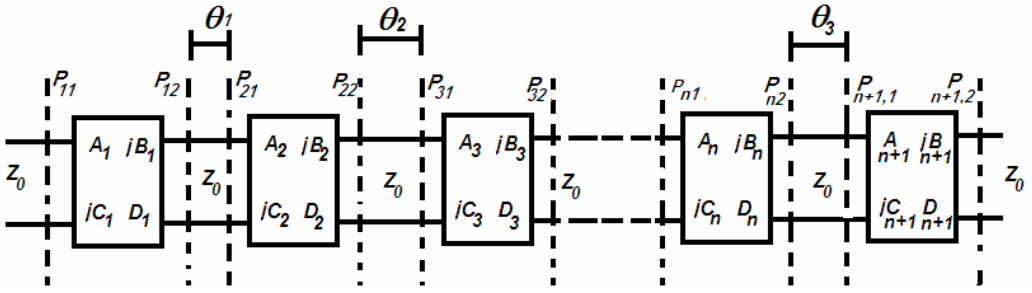

Fig. 4-21: Accurate network model including zeros of transmission. ABCD matrixes include information of the transmission zeros and behave as inverters at center frequency.

The products of the transfer matrix of Fig. 4-23 exhibit a Chebyscheff response in the in-band including also the information of the transmission zeros. Therefore, the final transfer function will be in the form:

$$T_{Total} = T_{Chebyscheff}(\omega).(\omega-\omega_1).(\omega-\omega_2).(\omega-\omega_3)....(\omega-\omega_n)..(\omega-\omega_{n+1})$$

where $\omega_1, \omega_2, \omega_3 ... \omega_n, \omega_{n+1}$ are the zeros of transmissions introduced by the coupling sections. In the specific case under consideration, these zeros appear between 120 and 140 GHz, with the consequence suppressing the TE102. Moreover, it is believed that the square coupling sections behave as stabs for the electromagnetic field [4-7], and this might justify the appearance of transmission zeros.

4.7. In-band improvements using "small-ridge"

Fig. 4-17 showed the in-band return loss better than 15.6 dB in frequency range of interest. This limit was "fixed" by the smallest length within the filter equal to 0.1 mm (the first coupling). In other words, if this length becomes smaller than 0.1 mm, a return loss as good as 25 dB can be achieved.

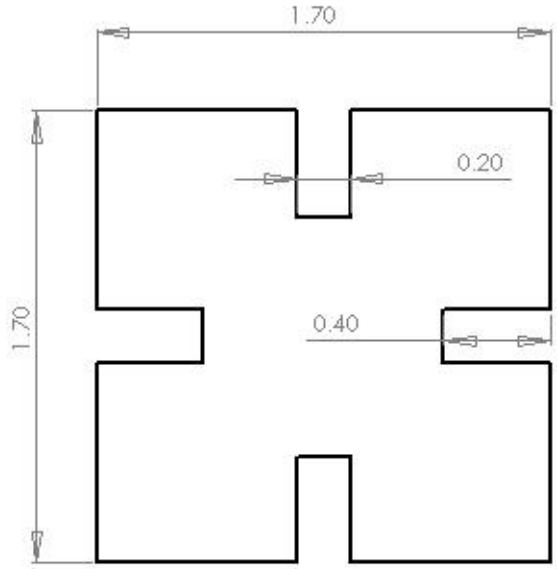

Fig. 4-22: In-band response of the 7-pole filter using a "small" ridge as first coupling section.

On the other hand, a smaller length translates into an impossibility of realizing physically the component. In this work, it is suggested to replace the first input coupling section with a different one. A similar approach was introduced in [4-4], where a coupling section has been exchanged with a ridge section with smaller ridge width. However in this work, the critical coupling section is replaced by a ridge section with smaller ridge lengths, fixing the ridge width. In the proposed design, the width of the ridge cannot be further reduced since its dimensions would become unrealizable.

The first square evanescent section is therefore substituted with a quadruple-ridge section under cut-off. Fig. 4-22 depicts the dimensions of the new ridge section in millimetres with cut-off frequency of the fundamental mode at 69.2 GHz. Since the field is concentrated in the

vicinity of the ridges, the introduction of a quadruple-ridge section makes a stronger coupling and it “relaxes” the coupling length. In conclusion, it is possible to achieve a 25 dB return loss with a minimum length of 0.2 mm (double that 0.1 mm) using this method. Fig. 4-23 shows the in-band return loss with the introduction of the “small” ridge in the first input coupling section.

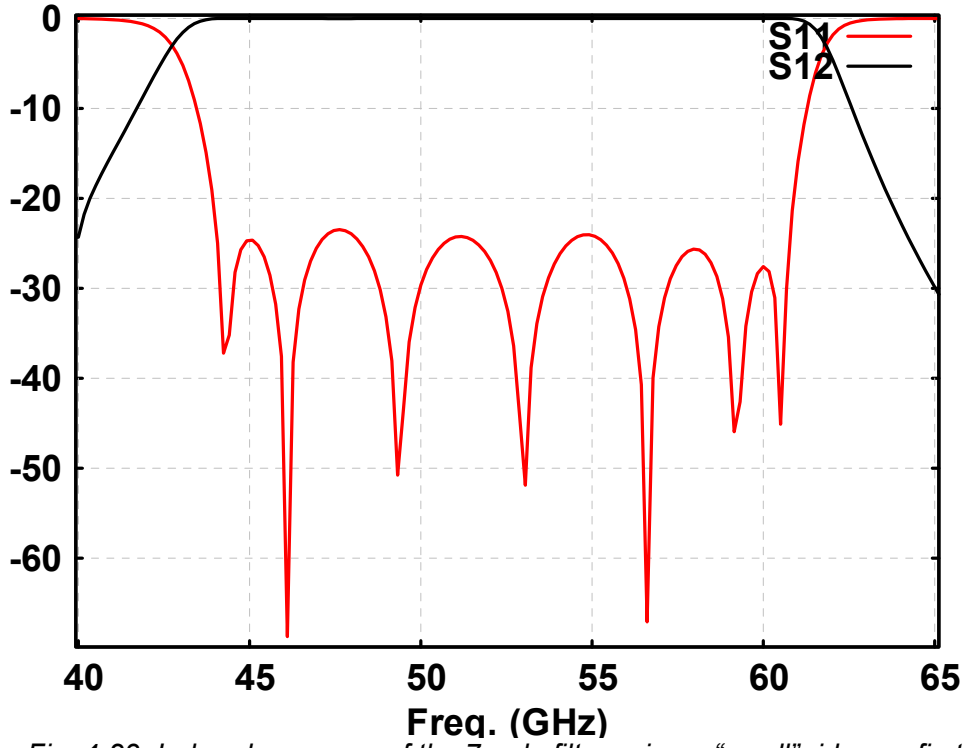

Fig. 4-23: In-band response of the 7-pole filter using a “small” ridge as first coupling section.

On the other hand, following what is mentioned above, by substituting the first evanescent section, two important zero of transmissions are lost. Therefore, the rejection in the frequency range of interest is supposed to deteriorate. Fig. 4-24 shows the response in a wider frequency range; it can be noted that the rejection got worse than is shown in Fig. 4-14.

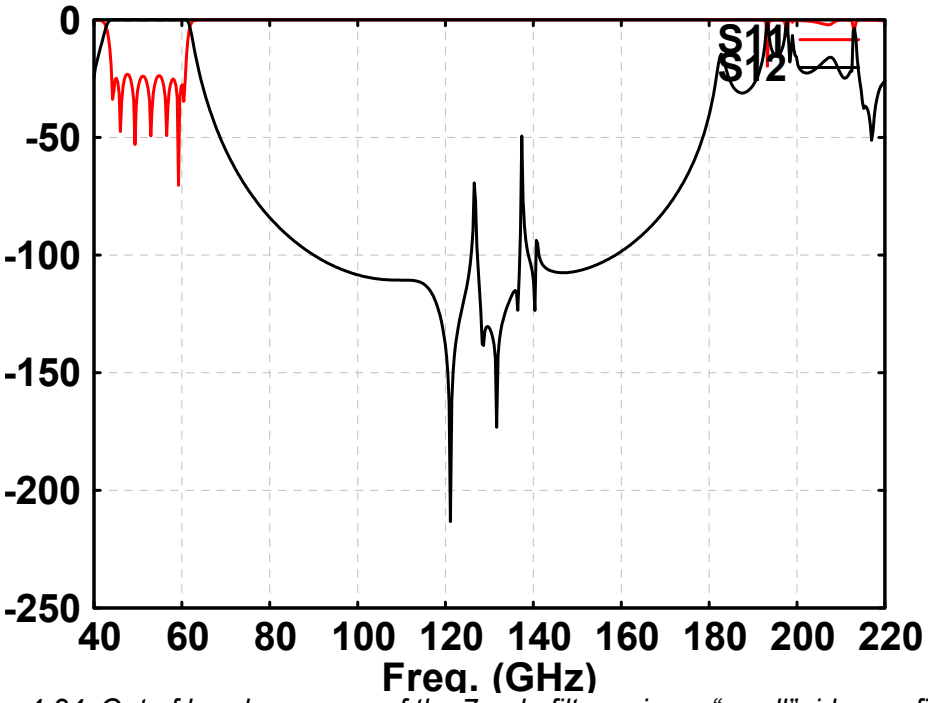

Fig. 4-24: Out of band response of the 7-pole filter using a "small" ridge as first coupling section.

4.8. Summary

Chapter 4 presented the quadruple ridge filter design. The cross-section has been introduced, and it maintains the four-fold symmetry requirement. The proposed filter uses seven poles, which accomplish the rejection requirements. Moreover, the important property of suppressing the repetition of the fundamental mode has been evidenced as an explanation of this phenomenon. The overall filter structure has been represented graphically along with plots of responses. Improvements in the in-band return loss are achieved by the usage of a quadruple "small ridge" section as the first evanescent section. The conclusions in chapter

4 confirm that the proposed quadruple ridge waveguide filter fulfils the RF specifications listed in chapter 3.

4.9. References

[4-1] Yu Rong, and Kawthar A. Zaki., "Characteristic of Generalized Rectangular and Circular Ridge Waveguides", IEEE Transactions and Microwave Theory and Techniques, Vol. 48, No. 2, February 2000

[4-2] Dr. A. M. K. Saad, COM DEV Ltd. 155 Sheldon Drive, Cambridge, Ontario, Canada, N1 R 7H6, "Novel lowpass harmonic filter for satellite application".

[4-3] Felice Maria Vanin, Dietmar Schmitt, Ralph Levy, "Dimensional Synthesis for Wideband Wave Guide Filters", IEEE International Microwave Symposium, Fort Worth, Texas (US), June 2003.

[4-4] Yu Rong, and Kawthar A. Zaki, John Gipprich and Daniel Stevens, "LTCC Wide-Band Ridge-Waveguide Bandpass Filters", IEEE Transaction on Microwave Theory and Techniques Vol. 47, NO. 9, September 1999.

[4-5] R. Levy, "A generalized design reciprocal technique for practical distributed ladder networks," IEEE Trans. Microwave Theory Tech., vol. MTT-21, pp. 519–526, Aug. 1973.

[4-6] Felice Maria Vanin, Dietmar Schmitt, Ralph Levy. "Dimensional Synthesis for Wideband Wave Guide Filters and Diplexers", IEEE Transaction, November 2004.

[4-7] Smain Amari, and Jens Bornemann, "Design of polarization-preserving circular waveguide filters with attenuation poles", Microwave and optical technology letters Vol.31, No.5, December 5 2001

Chapter 5 – Transformer and assembly

Though the proposed filter fills the requirements and satisfies the issue of handling both polarization states of the electromagnetic field, the frequency response of the filter must be tested using a standard waveguide. The standard waveguide WR 19 (4.775X2.388 mm) has an operative frequency between 40GHz and 60GHz, which coincides with the specifications of the proposed filter. However, NASA has provided a WR 19 with the dimensions of 4.775x4.775 mm that will serve as a standard for testing the unique quadruple ridge waveguide filter, allowing for the preservation of four-fold symmetry. The approach used in NASA/GSFC for test purposes is not conventional. In fact, it is required to test the whole science instrument from 40 GHz until 700 GHz at cryogenic temperatures. No network analyzer can handle such a wide frequency range. NASA is intended to measure the radiation pattern of the filter connected to a horn and then “derive” the S-parameter behavior. No other information can be given regarding the measurement system used in NASA for those frequency ranges. This chapter will focus attention on a novel transformer used to adapt the filter to square waveguide.

5.1. Transformer requirements and design concept

A link between the filter and the WR 19, a transformer, is necessary in order to allow measurements of frequency response that can be tested against a standard. The transformer must maintain the same symmetry employed in both the WR 19 (4.775x4.775 mm) and the proposed filter.

The summary requirements of the transformer are:

- Bandwidth: 40 – 60GHz
- Return loss: $\geq$ 20dB within bandwidth
- Transform filter cross-section into: 4.775x4.775 mm

Many transformer structures have been considered during the development of this work; e.g., the cascade of several square waveguides without ridges and cascade of non-uniform quadruple ridge cross sections, but these transformer structures did not achieve the requested bandwidth (from 40 to 60 GHz). Each study of alternative cross-sections required tedious and long electromagnetic simulations due to the calculation of coupling integrals. The main time consumption during simulation occurs when the electromagnetic engine of the software has to numerically calculate the propagating modes in the structure. Using non-uniform quadruple ridge waveguides, it is become clear that each individual

section has its own operative frequency and achievable bandwidth. Therefore, the physical limitations in terms of achievable bandwidth and return loss of the considered structures excluded them from use with the proposed filter.

5.2. Transformer design

The singular way to achieve the requested bandwidth is to connect the filter directly to the 4.775x4.775 mm housing rather than tapering the cross-section in several steps. While it was first assumed that a housing closer to the dimension of the filter should be used, simulation results confirm that the bigger the square housing that is used, the wider the achievable bandwidth will be. Network theory states that connecting two ports with different impedance ratios must be progressive and not abrupt. In this case, the impedance ratio between the filter and the WR 19 is 7 (as confirmed through simulations with a commercial software tool). This impedance ratio is extremely high. Therefore, the only method to preserve the bandwidth while matching the impedance (achieve the requested return loss) is by introducing tapered ridges within the transformer. The tapering progressively matches the impedances between the WR 19 and the proposed filter. In addition to this concept, there is still the requirement of maintaining four-fold symmetry, which led the design of the cross-section in the direction of using four ridges.

As shown in Fig. 5-1 and as previously stated, the transformer design has been achieved by directly connecting the filter to the housing and using appropriate tapering of the quadruple-ridges.

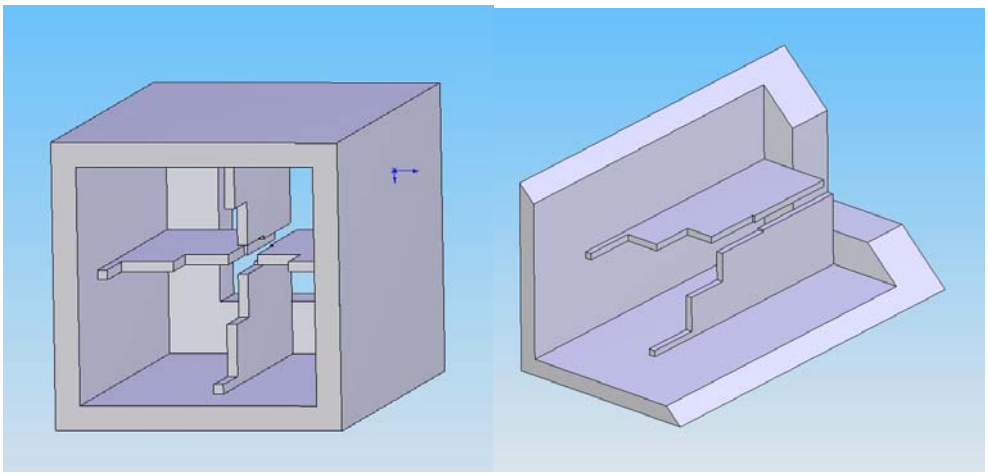

(a) (b)

Fig. 5-1: 3D drawings of the transformer. (a) Transformer structure, (b) longitudinal section of the transformer with cut plane at 45 degree angle.

The transformer in-band response is good. In order to realize and even better return loss, 30dB, additional tapered ridges should be used within the transformer. Fig. 5-2 shows the S parameter response of the transformer. There is a noticeable similarity to the S parameter response of a low pass filter.

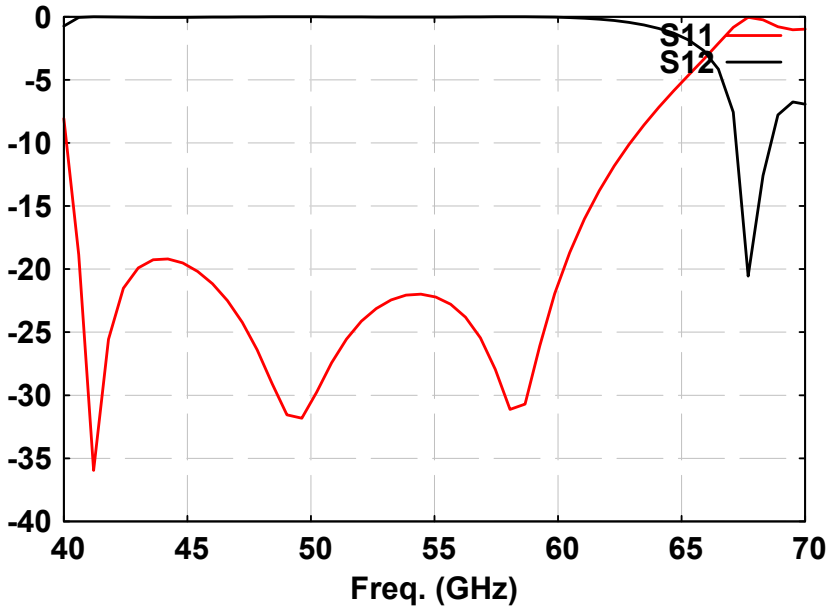

Fig. 5-2: In-band S-parameter response of the transformer.

As depicted in Fig. 5-3, the wide range response also conforms to bandwidth requirements. However, it is evident that outside of the bandwidth, the return and insertion losses do not behave ideally. In fact, after 65GHz the square rectangular waveguide it is not mono-mode anymore. In other words, it is like looking “outside” the natural operative frequency range of the transformer. The behavior of the structure after 65 cannot be trust anymore. Just for information, Fig. 5-3 shows that many spurious modes are introduced in the out-of-band frequency range. When the structures are assembled, the filter will eliminate the spurious modes and guarantee desirable rejection. However, a mono-mode structure between 40 and 200 GHz, e.g. coaxial connector or probe, shall be connected to the square waveguide in order to see in simulation only one mode. The connector or probe, which will behave as input/output, will “collect” all the energy of the other modes into the fundamental one. This

translates into appropriately exciting the structure and looking at the filter response together with the transformer.

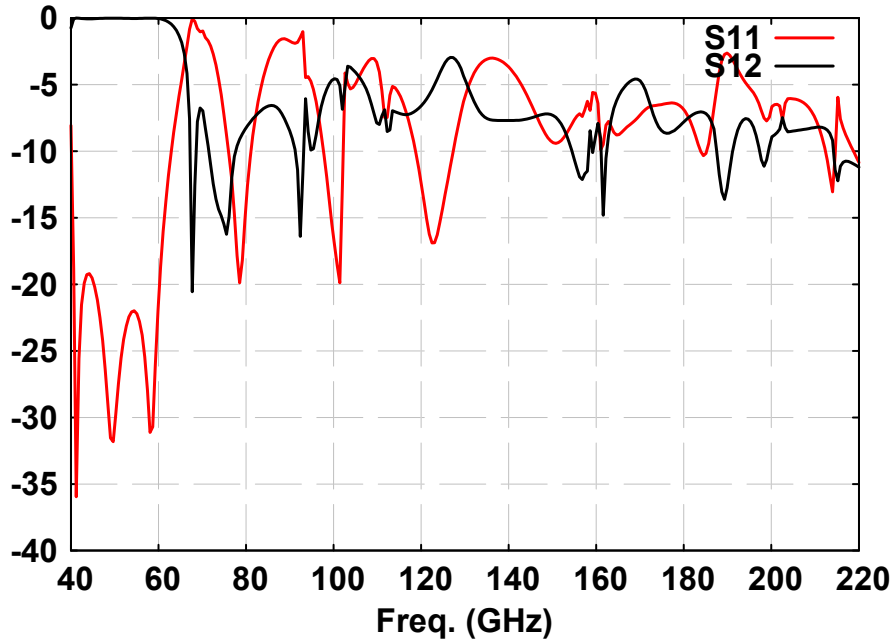

Fig. 5-3: Out-of-band S-parameter response of the transformer.

Because the response of the transformer matches the requirements of proposed filter, the last step is to assemble the filter and transformer.

5.3. Filter and transformer assembly

Fig. 5-4 depicts a longitudinal 3D drawing of the filter and the transformer together. Fig. 5-5 shows a closer detail of the connection between the filter and the transformer. The input (and output) waveguide length of the filter can be chosen arbitrarily.

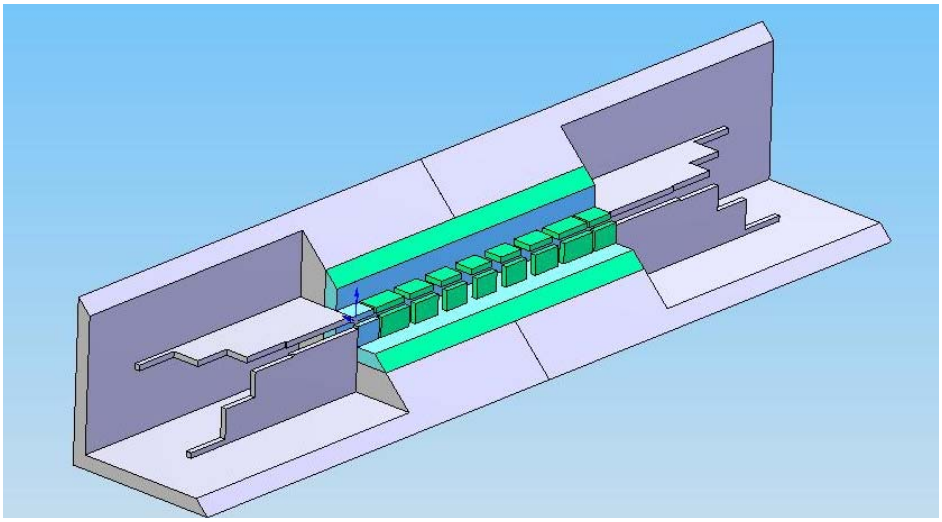

Fig. 5-4: Assembly between the filter and the transformer with cut plane at 45 degree angle.

In fact, it does not impact the return loss between the transformer and the filter in absolute value, but only in phase value.

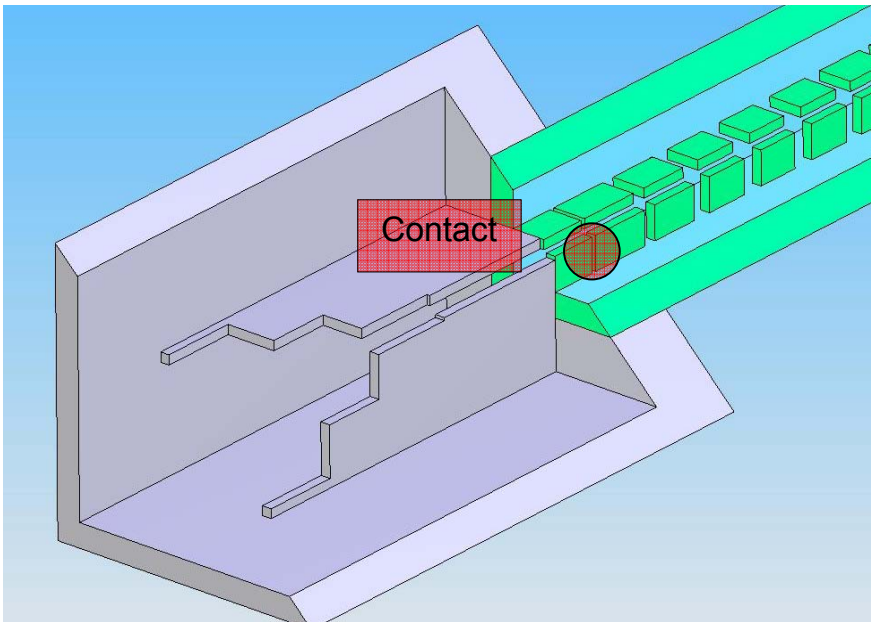

Fig. 5-5: Detail of the connection of the filter to the transformer with cut plane at 45 degree angle.

The in-band simulation of the structure, filter and transformer, response is given in the Fig. 5-6. This S-parameter can be still optimized achieving a better filter response.

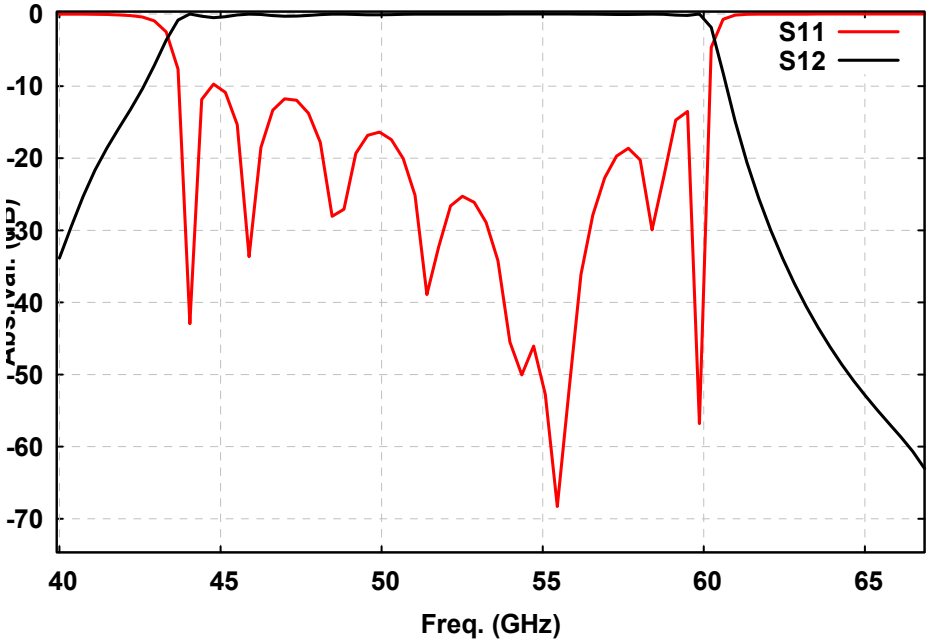

Fig. 5-6: In band S-parameter response of the structure filter plus transformer.

The response of the structure from 40 until 200 GHz is given in Fig. 5-7.

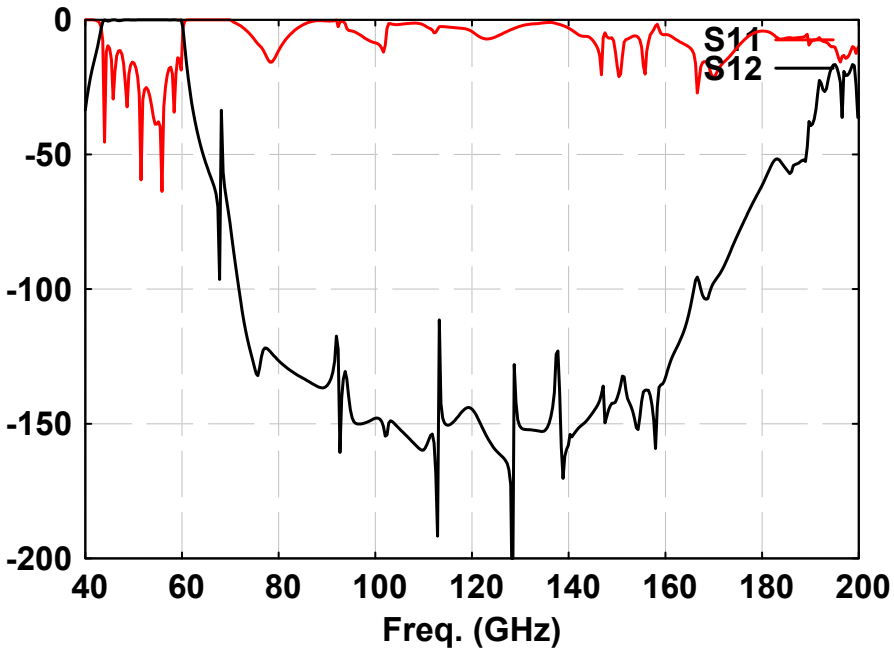

Fig. 5-7: Out-of-band S-parameter response of the structure filter plus transformer.

It is evident that the transformer introduces spikes in the out-of-band frequency range due to the modes excited in the larger waveguide. It is worthy to note that the spikes are real but fictitious, in fact as already mentioned they are due to the fact the rectangular waveguide is not mono-mode until 200 GHz. If a mono mode probe is introduced, this would collect the energy of the higher order mode into the fundamental one. Therefore, investigation and eventual improvements shall still be carried on. Finally, a drawing including mechanical dimensions is given in the Fig. 5-8.

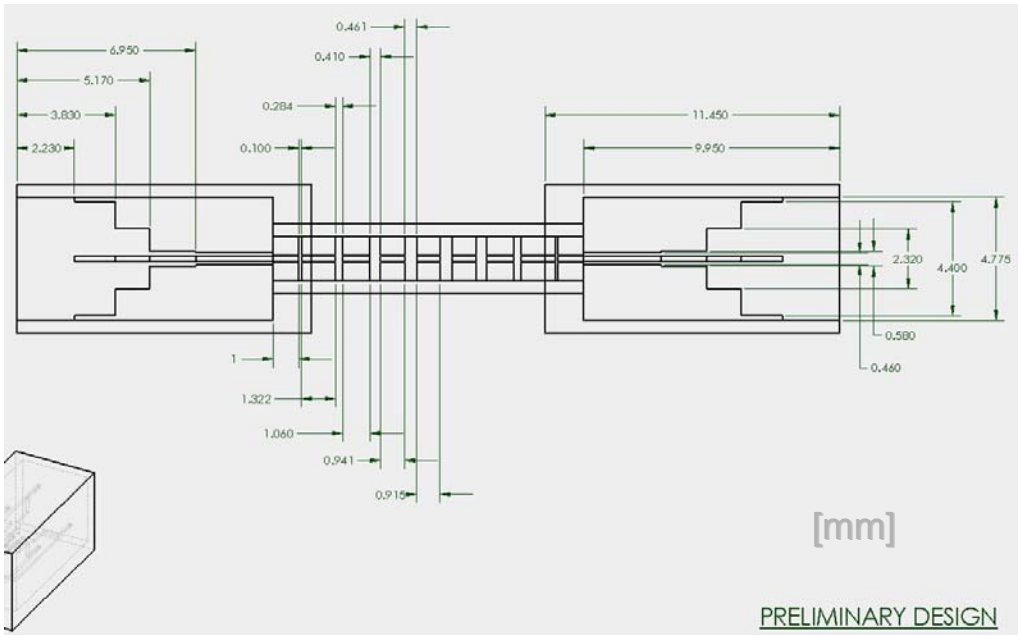

Fig. 5-8: Dimensions of the transformer assembled to the filter (dimensions are in mm).

5.4. In-band improvements using "small-ridge"

It has been shown (Fig. 5-6) that the in-band return loss is better than 10 dB after combining the filter with the transformer. However, the return loss can be significantly improved using the filter with the "small-ridge" discussed in the previous chapter and re-optimizing the whole structure. Following this approach and some optimization, Fig. 5-9 depicts the latest in-band filter response. It is worthy to note that the transformer structure introduces additional poles in the in-band. The return loss improvement is significant and acceptable.

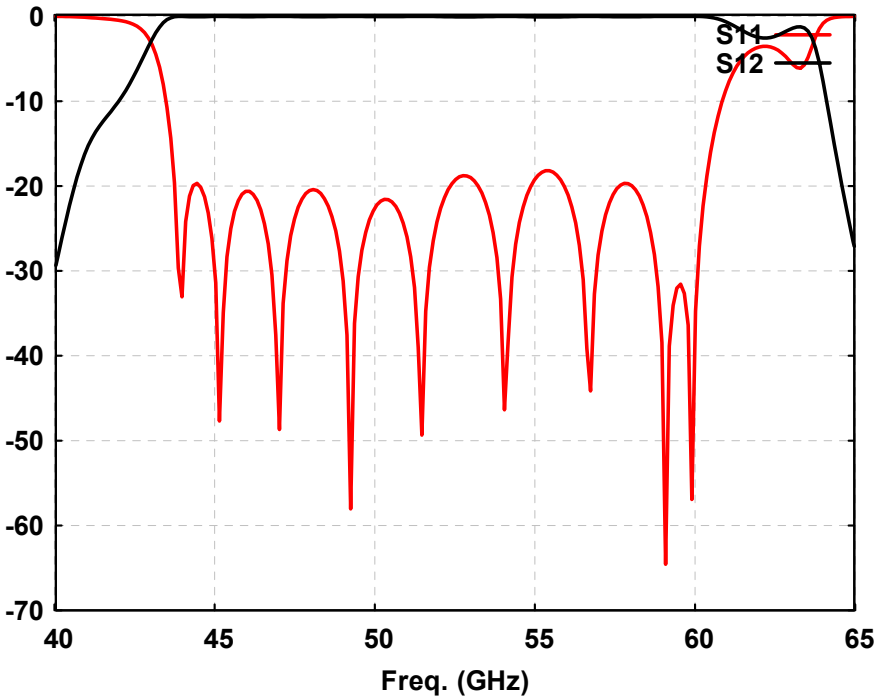

Fig. 5-9: In band S-parameter response of the structure filter plus transformer.

5.5. Possible excitation for different operative frequency ranges

In this work, it has often been mentioned that the frequencies of interest for the proposed structure are between 40 and 200 GHz. It is evident that there is not a conventional way to measure this filter for such high frequencies. Moreover, standard connectors or network analyzers able to measure the filter response between 40 and 200 GHz are, to my knowledge, unrealized. NASA/GSFC has developed their own “in-house” systems able to measure the filter presented in this work. NASA/GSFC will use a special method that cannot be described in this work because of reserved rights. Therefore, the filter design presented in this work concludes with the transformer between quadruple ridge waveguide and square 4.775x4.775 mm housing.

However, some possible solutions are now considered for different operative frequency ranges e.g. C or L band. Two possible excitations will be now discussed:

1. Excitation using OMT (orthomode transducer) and standard rectangular waveguides.
2. Excitation using square housing with coaxial probes.

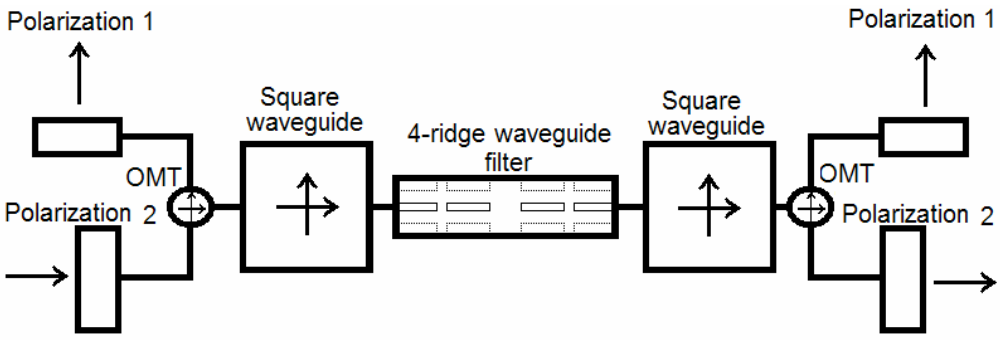

Fig. 5-10: Excitation using OMT and standard rectangular waveguides.

Fig. 5-10 shows a system using two OTMs to excite the structure. Because of the structure's symmetry, the orthogonal polarizations are separated and they can be treated at the same time from input to output. The excitations are performed using standard rectangular waveguides or by connecting a standard connector to the rectangular waveguide.

The second approach is the excitation of the square transformer with two coaxial probes simultaneously at each port as Fig. 5-11 depicts. Port A will couple with port B, and port C will couple with port D; in fact,

also in this case the two symmetries will not enable coupling between the two orthogonal modes. Fig. 5-11 portrays only the square housing, not the filter or transformer.

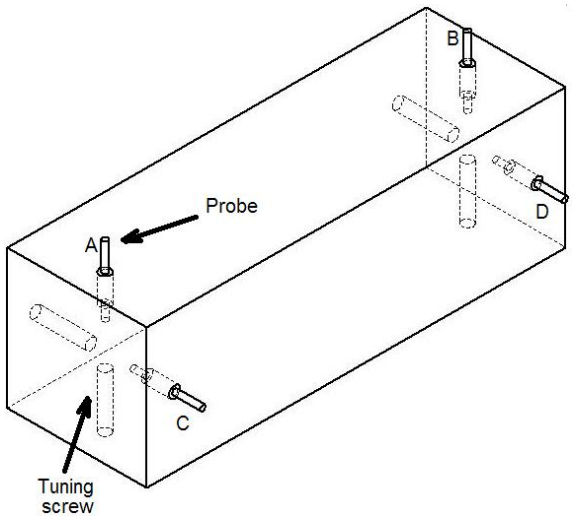

Fig. 5-11: Excitation using probes into a square cavity. Probes, and tuning screws, and A B C D ports are in evidence.

A qualitative picture that shows the two filters inside the square housing is shown in Fig. 5-12, where the two pole filter (without transformer) is now shown within the structure.

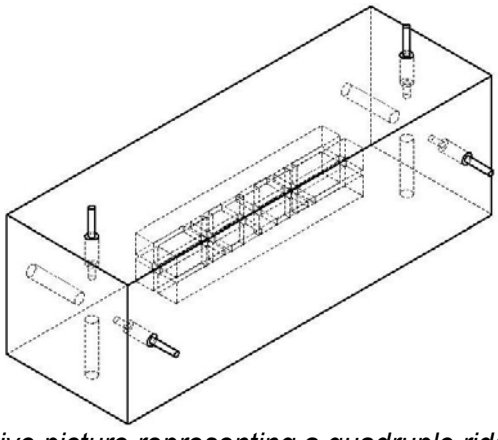

Fig. 5-12: Qualitative picture representing a quadruple ridge waveguide filter excited with probes.

5.6. Summary

In the beginning of this chapter, the requirements for connecting the transformer to the filter with square WR 19 were described. Possible transformer designs were investigated and development of an appropriate tapered quadruple ridge design was then described. The assembly of the proposed filter and transformer has been depicted through images and description, and the response was also explained. Clarifications of the "spikes" introduced by the transformer have also been given. The dimensions of the structure are shown with a mechanical drawing. Finally, it is shown that significant in-band return loss is improved by replacing the first (and the last) square evanescent sections with a quadruple ridge section under cut-off and by re-optimizing the whole structure. Possible input-output excitations for filters operating at lower frequencies are also discussed at the end of the chapter.

Chapter 6 – Applications, conclusions, and outlook

NASA Science efforts are concentrated in answering humanity's deepest questions, such as how the universe came into being, how stars, galaxies, and planets began their lives and whether there is life on other worlds. The Beyond Einstein Program represents NASA efforts to explore the ultimate extremes of nature including the birth of the universe. Part of the process of dating the universe is the accurate measurement of the Polarization of the Cosmic Microwave Background (CMB), which is the focus of the next NASA mission. A new generation of science instruments dedicated to the CMB has been under development at NASA since 2002.

New microwave components are a necessary part of the course of instrument development. The research for these components is testing limits of current technology with extreme RF requirements. In this work, a novel waveguide filter structure has been introduced and presented. For the first time, a filter has been realized using a quadruple ridge cross section, which has the property of exhibiting four-fold symmetry and at the same time controlling the appearance of higher order modes. The four-fold

symmetry is necessary for the preservation of the field polarization. The ridges are used in order to shift the second propagating mode far away in frequency. By using this cross section, a large spurious free frequency range can be achieved. With the appropriate cross section design, the fundamental mode can be fixed at 40 GHz and the second propagating mode as high as 200 GHz. It has been shown that by using a quadruple ridge cross-section Chebyscheff filters are realizable when appropriately cascading quadruple waveguide sections are separated by evanescent waveguides.

This work has discussed the phenomenon of the fundamental mode repetition typical of filter designs. It has been shown that using this cross-section with an appropriate number of evanescent cross sections, the repetition of the fundamental mode can be suppressed. In fact, each evanescent cross section that separates the quadruple waveguides introduces a zero of transmission such as that the sum of the zeros totally suppresses the filter repetition.

For the particular design under consideration, a broadband design of 30% fractional bandwidth has been requested. The extreme fractional bandwidth reflects into strong couplings, which translate into very small coupling section lengths. These lengths can be as small as 0.1 mm, which represents a physical limit for practical realizations. It has been shown that

in order to improve the in-band return loss, these lengths shall be even smaller than 0.1 mm. However, smaller lengths are not realizable with current technology. In this work, it has been shown that by substituting the first square evanescent section (the smallest section) with a quadruple ridge section under cut-off, in-band return loss of 25 dB is achieved. Moreover, the smallest coupling section length has been double to 0.2 mm from 0.1 mm, at the price of slightly deteriorating the stop-band performances. Finally, novel transformer geometry has been introduced and designed keeping the property of the four-fold symmetry. The transformer converts the cross-section of the filter into square WR 19.

In conclusion, the filter design presented in this work has the property of preserving the dual polarization state of the electromagnetic field, guaranteeing wide bandwidth and at the same time exhibiting a very wide stop-band frequency range. Our current knowledge indicates that other structures showing the same performances in one single component are not known. Therefore, this device represents the state of the art in terms of polarization preservation waveguide filter while offering at the same time an extremely wide stop-band frequency range. In other words, this filter exhibits the properties of ridge waveguide filter but preserves the two polarization states of the electromagnetic field.

The main limits of the structure are identified into the power handling and in manufacturing the four-fold symmetry. In fact, the power

handling depends on the distance among the four ridges, which is small in practical applications. The symmetry is essential in allowing for the correct functioning of the filter.

This filter structure finds applications in systems where coherent signal processing is an issue and therefore preserving the field polarization is a need. It is believed that, in several applications, the usage of orthomode transducers (OMT) can be avoided. OMTs separate the two polarizations in two different channels, which are often followed by filters. Therefore, each channel processes the polarization individually through the use of several components. On the other hand, using the proposed structure creates the possibility of using one single element, which saves mass, volume, additional components, and costs.

Looking at the future, possible extensions are already foreseen; for example, preserving quadruple ridge waveguide filters with attenuation poles on the close side of the bandwidth [3 6], dual mode applications, and also polarization preserving diplexers. Moreover, possible excitations for different frequencies such as C, L, Ku or Ka band shall be also investigated.

The design of this filter is a contribution to the vast engineering research world. With this work, an additional step has been made in

improving current technology not only for space application, but also for terrestrial, defence, communication applications, and applied sciences.

References

[2-1] W. P. Mason and R. A. Sykes, “The use of coaxial and balanced transmission lines in filter and wide band transformers for high radio frequencies”, *Bell Syst. Tech. J.*, vol. 16, pp. 275-302, 1937.

[2-2] G. L. Matthaei, L. Young, and E. M.T. Jones, *Microwave Filters, Impedance-Matching Networks and coupling Structures*, New York: McGraw-Hill Book Co., 1964

[2-3] S.B. Cohn, “Direct- Coupled- Resonator Filters”, Proceedings of the IRE, vol. 45, pp. 187-196, February 1957.

[2-4] R. Levy, “Theory of Direct Coupled Cavity Filters”, IEEE Transaction on Microwave Theory and Techniques vol. MTT-11, N0. 6, pp. 340-348, June 1967

[2-5] G. Conciauro, M. Guglielmi, R. Sorrentino, *Advanced Modal Analysis,* New York: John Wiley & Sons, LTD 1999

[3-1] A.M. Boifot, E. Lier, T. Schaug-Pettersen, “Simple and broadband orthomode transducer” IEE proceedings, Vol. 137, Pt, H, No. ^,December 1990.

[3-2] G. Chottopadhyay, B. Philhour, J. Carlstrom, S. Church, A. Lange, and J. Zmuidzinas, “A 96-GHz Ortho-Mode Transduced for the Polatron”, IEEE Microwave and Guided Wave Letters Vol. 8, No. 12 December 1998

[3-3] N. Yoneda, M. Miyazaki, T. Noguchi, “A 90GHz –Band Monoblock Type Waveguide Orthomode Transducer”, IEEE MTT-S Digest 1999

[3-4] M.P. Natarov, L.A. Rud, V.I. Tkachenko, “Orthomode Transducer for mm-wave range”, MSMW’04 Symposium Proceedings. Kharkov, Ucraine, June 21-26, 2004

[3-5] Chung-Li Ren, and Han-Chiu Wang “H01 circular waveguide low-pass filter for millimeter wave transmission system”

[3-6] Smain Amari, and Jens Bornemann, “Design of polarization-preserving circular waveguide filters with attenuation poles”, Microwave and optical technology letters Vol.31, No.5, December 5 2001

[3-7] K. U-yen, E. J. Wollack, T. Doiron, J. Papapolymerou, and J. Laskar, “The Design of a Compact, Wide Spurious-free Bandwidth Bandpass Filter Using Stepped Impedance Resonators,” accepted to the IEEE 8th European Microwave Conf., Paris, France, October, 2005.

[3-6] K. U-yen, E. J. Wollack, T. Doiron, J. Papapolymerou, and J. Laskar, “A Bandpass Filter Design With Extended Rejection Bandwidth Using Double Split-end Stepped Impedance Resonators, “ to be submitted to IEEE Microwave Theory Tech., July 2006.

[3-9] Felice Maria Vanin, Dietmar Schmitt, Ralph Levy, “Dimensional Synthesis for Wideband Wave Guide Filters”, IEEE International Microwave Symposium, Fort Worth, Texas (US), June 2003.

[4-1] Yu Rong, and Kawthar A. Zaki., “Characteristic of Generalized Rectangular and Circular Ridge Waveguides”, IEEE Transactions and Microwave Theory and Techniques, Vol. 48, No. 2, February 2000

[4-2] Dr. A. M. K. Saad, COM DEV Ltd. 155 Sheldon Drive, Cambridge, Ontario, Canada, N1 R 7H6, “Novel lowpass harmonic filter for satellite application”.

[4-3] Felice Maria Vanin, Dietmar Schmitt, Ralph Levy, “Dimensional Synthesis for Wideband Wave Guide Filters”, IEEE International Microwave Symposium, Fort Worth, Texas (US), June 2003.

[4-4] Yu Rong, and Kawthar A. Zaki, John Gipprich and Daniel Stevens, “LTCC Wide-Band Ridge-Waveguide Bandpass Filters”, IEEE Transaction on Microwave Theory and Techniques Vol. 47, NO. 9, September 1999.

[4-5] R. Levy, “A generalized design reciprocal technique for practical distributed ladder networks,” IEEE Trans. Microwave Theory Tech., vol. MTT-21, pp. 519–526, Aug. 1973.

[4-6] Felice Maria Vanin, Dietmar Schmitt, Ralph Levy. “Dimensional Synthesis for Wideband Wave Guide Filters and Diplexers”, IEEE Transaction, November 2004.

[4-7] Smain Amari, and Jens Bornemann, “Design of polarization-preserving circular waveguide filters with attenuation poles”, Microwave and optical technology letters Vol.31, No.5, December 5 2001

Felice Maria Vanin

F.vanin04@fulbrightweb.org

Education:

09/05-Present

Admitted to the PhD program in Electrical Engineering at the University of Maryland U.S.A. Completed course requirements for the PhD.

09/04-12/05

MS Degree in Electrical Engineering at the University of Maryland U.S.A. under FULBRIGHT program. Graduation in December 2005. GPA 3.8.

Title of the thesis: "Polarization-preserving waveguide filter for astronomical applications."

Academic advisor Prof. Kawthar Zaki full professor of Electrical Engineering.

Courses Include: Satellite Design and Spacecraft Communications.

1996-2002

MS Degree in Electronic Engineering at "La Sapienza University" of Rome. Title of the thesis: "Dimensional synthesis for rectangular inductive iris filters."

Academic advisor Prof. Fabrizio Frezza, full professor of Electromagnetic Field.

.

Professional Experiences:

09/05-Present Research Assistant

University of Maryland, United States of America

- Simulated, analyzed, and designed microwave components. Supported the research activities of the department and collaborated with NASA experts.

06/05-09/05 Intern in NASA/Goddard Space Flight Center

Microwave Instrument Technology Branch NASA/Goddard Space Flight Center

- Supported the Observational Cosmology Laboratory in NASA.
- Addressed the performance needs for a cosmic microwave background polarization measurement science mission. Novel polarized measurements of the cosmic microwave background used to acquire more knowledge about the

universe. Designed and simulated a novel microwave component for astronomical applications.

- Collaborated with microwave experts to plan and revise the science instrument as necessary while acting as the liaison between technical personnel and department head.
- Title of the thesis: “Polarization-preserving waveguide filter for astronomical applications.”
- As a result of the microwave component a NASA patent is under consideration.
- Representing Observational Cosmology Laboratory Department head, presented original instrument design to the Microwave Technology Branch.

03/04-09/04 Contractor engineer in ESA/ESTEC

TEC-ETM section at the European Space Agency, ESA-ESTEC (Noordwijk, The Netherlands)

- Supported with a leading role in the design, development, and verification of filter units for the GALILEO GSTB-V2 project. Duties included tracking schedules, interfacing with industries, participating to technical meetings and missions, preparation of control documents.
- Prepared, defined, and established contracts with specifications for TRP and GSTP, with additional experience in the finalization and monitoring of these contracts.
- Supported and prepared ARTES proposals for microwave techniques and technologies; such as, high power dielectric filters and loss reduction in microwave passive components.
- Developed and supported ESA software simulation tool FEST3D, contributing to the improvement of FEST3D as a simulation as well as a design tool.

01/03-03/04 ESA-ESTEC Research Fellow

Microwave field within the “Research and Training Network” funded by the European Union

- Interacted with European research institutes during the support of FEST3D. Collaboration with these research institutes promoted personal understanding of the strengths and weaknesses within the microwave field in Europe in terms of software simulation tools.
- Developed and implemented the “MAGIC TOOLS” in FEST3D for automatic designs of microwave passive components, such as bandpass, lowpass filters and diplexers. “MAGIC TOOLS” now represent the highest improvement in the FEST3D software tool.

11/02-present Collaborator

Department of Electromagnetism of the faculty of Electronic Engineering, "La Sapienza University" of Rome

- Researched activities in electromagnetic field.
- Assisted in teaching courses in the microwave field.
- Followed graduate students during their final thesis production.
- Revised IEEE publications.

04/02-11/02 Student Intern at ESA-ESTEC.

- Title of the thesis: "Dimensional Synthesis for Rectangular inductive iris filters"
- As a result of this thesis I achieved the maximum mark and IEEE publication.
- Final presentation held in ESA in the section TEC-ETM.

Publications & Patents:

08/05 NASA patent pending for microwave design.

01/05 "Automatic Dimensional Synthesis Without Optimization for Stepped Impedance Low-Pass Filters" M. Simeoni, S. Cacchione, F. Vanin, J. Molina Perez and D. Schmitt, Microwave and Optical Technology Letters.

11/04 "Dimensional Synthesis for Wideband Wave Guide Filters and Diplexers", Felice Maria Vanin, Dietmar Schmitt, Ralph Levy. IEEE Transaction.

06/04 "Dimensional Synthesis for Wideband Wave Guide Filters", Felice Maria Vanin, Dietmar Schmitt, Ralph Levy, IEEE International Microwave Symposium, Fort Worth, Texas (US).

06/04 "Dimensional Synthesis of Rectangular Waveguide Filter Types Without Optimization", D. Schmitt, F. Vanin, M. Simeoni, J. Molina Perez, R. Levy, IEEE Workshop on Comparison of Modern Filter Design Techniques: Design Fusion, End the Confusion, Fort Worth (TX).

05/04 "FEST3D – Novel Automatic Passive Component Design Tool", M. Simeoni, F. M. Vanin, J. A. Molina Perez and D. Schmitt, Microwave Technology and Techniques Workshop – Preparing for Future Space Systems, European Space Research and Technology Centre (ESTEC), Noordwijk, The Netherlands.

Scholarships:

2004/2005 FULBRIGHT AWARD of $20,000 for the academic year 2004/2005

- Sponsored by the US Department of State for the promotion of international relations.
- Award applies to the study of electrical engineering at the University of Maryland.

2004/2005 Tuition Scholarship Award of $22,000 in the University of Maryland

- Waives tuition cost exceeding FULBRIGHT scholarship award.

2002 Scholarship in "La Sapienza University" of Rome

- Awarded as a result of the highest grades in the Electronic Engineering Department.
- Allowed for completion of Master's thesis abroad in ESA-ESTEC.

2001 & 2002 Two Scholarships in "La Sapienza University" of Rome

- Awarded as a result of the highest grades in the Electronic Engineering Department.
- Duties included lab research assistance in the Electronic Engineering Department.

Membership:

IEEE member

Member of the Fulbright Alumni Association

Engineering Chapter University of Maryland Alumni Association

Skills:

Languages:	English: Fluent Italian: Mother tongue
Software:	Microsoft Office Tools, Lotus Notes, Mathematica, HFSS, CST Microwave Studio, FEST3D, EM-Design Software, Programming Languages: FORTRAN 77-90, Turbo Pascal 7.0, C, Assembler, MATLAB, VHDL.
IT skills:	Operating Systems: Windows 2000/XP, Linux, Solaris

Interests:

Music, travelling, photography, art, lecture, tennis, basketball, and boxing.

References:

Dr. Edward J. Wollack, NASA/Goddard Space Flight Center, Science staff
E-mail: Edward.J.Wollack@nasa.gov
Tel :+1-301-286-1379

Dr. Dietmar Schmitt, ESA-STAFF, project leader Artes4.
E-mail: Dietmar.Schmitt@esa.int
Tel: +31- (0)71-5653534

Luciano Balestra, ESA-STAFF, progect manager Galileo GSTB-V2.
E-mail: Luciano.Balestra@esa.int
Tel: +31- (0)71-5653676